CDF/DOC/BOTTOM/CDFR/8085
February 6, 2006 - Version 0.0

$Br(B_s \to D_s D_s)/Br(B^0 \to D^+ D_s)$ $D_s \to \phi\pi(3\pi, K^*K), \quad D^+ \to K\pi\pi$ with $355pb^{-1}$ in Run II

B. Iyutin, Ch. Paus

Massachusetts Institute of Technology

Abstract

We conducted a study of the ratio of the branching fractions $\frac{Br(B_s \to D_s^+ D_s^-)}{Br(B^0 \to D_s^+ D^-)}$ where $D_s \to \phi\pi(K^*K, 3\pi)$, $D^+ \to K\pi\pi$. and measured:

$$\frac{f_s}{f_d} \frac{Br(B_s \to D_s^+ D_s^-)}{Br(B^0 \to D_s^+ D^-)} = 1.00 \pm 0.24(Stat) \pm 0.06(Syst) \pm 0.23(Br)$$

$$\frac{Br(B_s \to D_s^+ D_s^-)}{Br(B^0 \to D_s^+ D^-)} = 3.84 \pm 0.93(Stat) \pm 0.24(Syst) \pm 0.56(f_s/f_d) \pm 0.90(Br)$$

1 Introduction

This note is a report on our first observation of $B_s \to D_s^+ D_s^-$ at CDF. $B_s \to D_s^+ D_s^-$ has a pure CP even final state and $B_s \to D_s^{(*)+} D_s^{(*)-}$ has a predominantly CP even final state. These modes are the major contributors to the phase-space difference between the even and the odd B_s decay channels. Measuring the total branching fraction of double charm B_s decays should give an estimate for $\frac{\Delta\Gamma}{\Gamma}$.

$B_s \to D_s^+ D_s^-$ measurement is difficult due to the small branching fractions of charm meson decays available for full hadronic reconstruction.

To test our tools we use similar but more populated modes. To suppress systematics we study ratios of branching fractions. Several of them will give us a good handle to test and tune our techniques.

$$\frac{Br(B_s^0 \to D_s^+ 3\pi)}{Br(B^0 \to D^- 3\pi)}, \quad (D_s^+ \to \phi\pi(3\pi, K^*K), D^+ \to K\pi\pi) \tag{1}$$

$$\frac{Br(B^0 \to D_s^+ D^-)}{Br(B^0 \to D^- 3\pi)}, \quad (D_s^+ \to \phi\pi(3\pi, K^*K), D^+ \to K\pi\pi) \tag{2}$$

$$\frac{Br(B_s \to D_s^+ D_s^-)}{Br(B^0 \to D_s^+ D^-)}, \quad (D_s^+ \to \phi\pi(3\pi, K^*K), D^+ \to K\pi\pi) \tag{3}$$

$$\frac{Br(B_s \to D_s^+ D_s^-)}{Br(B_s^0 \to D_s^+ 3\pi)}, \quad (D_s^+ \to \phi\pi(3\pi, K^*K), D^+ \to K\pi\pi) \tag{4}$$

All the listed decay modes have six tracks in the final state and share similar topology with two secondary resonances decaying into three tracks each. In $B_s^0 \to D_s^+ 3\pi$ and $B^0 \to D^- 3\pi$ stand-alone pions are coming from a_1 decay treated in reconstruction as a resonance with no lifetime. Using the same D_s and D^+ decay modes allows to optimize reconstruction and analysis as well as reduce systematics.

This setup provides a lot of possibilities for crosschecks and additional studies. The first ratio is measured in [2]. The second ratio is measured in [1]. This note describes the measurement of the third and the forth ratios.

The reconstruction of $B^0 \to D^- 3\pi$ and $B_s^0 \to D_s^+ 3\pi$ modes is thoroughly studied in [2].The reconstruction of $B^0 \to D_s^+ D^-$modes is done in [1]. We are going to use the obtained results with minor changes where needed.

2 Data Samples and NTuple Production

The STN production was run simultaneously for several analyzes. It saved time and disk space since the same collections of D_s and D^+ candidates were used to reconstruct all the decays.

The production process is thoroughly described in [2]. For double-charm reconstruction we run through the collections of D-mesons and try to fit all the combinations of $B_s \to D_s^+ D_s^-$. $\pm 100 MeV$ windows are chosen for charm mesons. Their masses are constrained to PDG values when fitting B_s.

3 Monte Carlo Simulation

Here we again refer to [2]. Exactly the same techniques were applied to MC.

- Realistic simulation
- Run by run luminosity handling
- Trigger confirmation
- Run by run prescale
- Duplicates removal
- Self-reflection removal

We also would like to refer to the comparison between data and Monte Carlo performed in [2] for high statistics mode $B^0 \to D^- 3\pi$. There is no reason to repeat it for $B^0 \to D_s^+ D^-$ since the mode only contains several hundred events and comparison will not be statistically significant.

3.1 Efficiencies extracted from the Monte Carlo

For $B^0 \to D_s^+ D^-$ we generated 60×10^6 signal events with decay file quoted in table 1. For $B_s \to D_s^+ D_s^-$ we generated 60×10^6 signal events with decay file quoted in table 2. We scaled relative ratios of three different D_s decay modes and their products with the best knowledge of branching fractions from PDG. We applied detector simulation, trigger, reconstruction, run by run prescale the way it is described in [2].

To get a number of events we fitted signal Monte Carlo with signal templates and integrated the region containing 95.45% of the signal. Fit parameters are saved to use for signal template. $B^0 \to D_s^+ D^-$ signal fits are shown on figures 14, 15, 16 for `B_CHARM` on the left and `B_CHARM` and `LOWPT` combined on the right. $B_s \to D_s^+ D_s^-$ signal fits are shown on figures 17, 18, 19 for `B_CHARM` on the left and `B_CHARM` and `LOWPT` combined on the right. The final yield numbers for efficiencies are summarized in table 9 for $B^0 \to D_s^+ D^-$ and in table 11 for $B_s \to D_s^+ D_s^-$. The yield numbers and efficiencies for $B^0 \to D_s^{+(*)} D^{-(*)}$ modes are summarized in table 10.

4 Cut Optimization

We used several guidelines to choose our analysis cuts.

- Cut should have non trivial separation power between signal and background.
- Cut should be unique. It should reduce background unreachable by other cuts.
- We constrained ourselves by using signal Monte Carlo only therefore we can not use cuts which rely on the structure of underlying event i.e. any kind of isolation cuts.

The final values are chosen with a help of optimization procedure. It requires a lot of repetitive runs over data. For optimization we only use background on the right from the signal to avoid bias from misreconstructed decays on the left.

We fit mass distribution with a sum of flat and exponent. Monte Carlo effective signal width is used to estimate the extent of the blind region and the width of the signal for significance calculations.

The process is iterative. Each cut is varied within reasonable limits. While one cut is varied the others are fixed to default values. In the beginning, procedure applies default cuts to Monte Carlo and scales Monte Carlo yield to the expected number of signal candidates. The step by step algorithm is described below.

1. Fit MC signal with default cuts
2. Scale MC to expected signal yield
   (a) Change one cut while fixing the others at default values
   (b) Fit scaled MC signal, get the effective width
   (c) Chose blind region as $\pm 3.0\sigma$ of MC signal width
   (d) Fit Data with BG omitting the blind region
   (e) Integrate Data BG under $\pm 2.0\sigma$ signal region
   (f) Integrate scaled MC signal in the same $\pm 2.0\sigma$ region
   (g) Save significance
   (h) Go to next cut value
   (i) If done with the cut go to next cut
   (j) If done with all the cuts, - print results
3. The default cuts and variation windows could be changed according to results
4. The procedure could be started from the beginning

$B^0 \to D_s^+ D^-$modes with higher statistics were optimized with respect to Gaussian significance $Sig/\sqrt{(Sig + BG)}$ similar to what we did in [2] and [1]. $B_s \to D_s^+ D_s^-$ modes were optimized with Poisson significance. For this we fitted the background omitting the signal region and calculated the probability of the scaled Monte Carlo signal to be the background fluctuation. The final cut values were chosen to minimize that probability.

While running procedure shows a dynamic fit for visual quality check (figure 1). As an output it gives the efficiency and significance plots as functions of cut value for every varied cut. Figures 8 and 9 show the significance and efficiency curves for $B_s \to D_s^+ D_s^-, (\phi\pi)(\phi\pi)$, figures 10 and 11 show the significance and efficiency curves for $B_s \to D_s^+ D_s^-, (\phi\pi)(K^* K)$, figures 12 and 13 show the significance and efficiency curves for $B_s \to D_s^+ D_s^-, (\phi\pi)(\pi\pi\pi)$. The optimization plots for $B_s \to D_s^+ D_s^-, (\phi\pi)(\phi\pi)$shows an abrupt kink at the moment when the last background event in the $[5.2, 6.0]GeV$ region disappears. The jump of significance is not physical and exposes the approximate nature of our calculation of the optimization significance. The exact significance of the $B_s \to D_s^+ D_s^-$ resonance discovery is discussed later.

Procedure usually takes several iterations to converge. The final values for cuts are guidelined by efficiency and significance curves. We usually choose to cut at the maximum of the significance. If significance distribution has a plateau the cut is set in the beginning of the plato. $B^0 \to D_s^+ D^-$modes optimization includes five L_{xy} related cuts which are highly correlated but also remove unique backgrounds. Due to several correlated cuts optimization procedure could converge to several different optimal set of cuts. We had to chose one which we considered the most significant. The final results are summarized in tables 3 and 4. Despite the fact that `B_CHARM` and `LOWPT` samples have the same analysis cuts the implicit trigger cuts are different.

5 Templates for Signal and Background.

The background fitting model affects the quality of the total fit and may significantly change the estimated signal. Earlier analysis [3] shows that fitting model gives one of the largest inputs into systematics.

5.1 Signal Templates.

We use multiple Gaussians to fit our signals. $B^0 \to D_s^+ D^-$and $B_s \to D_s^+ D_s^-, (\phi\pi)(K^* K)$signals are fitted with double Gaussian. $B_s \to D_s^+ D_s^-, (\phi\pi)(\phi\pi)$and $B_s \to D_s^+ D_s^-, (\phi\pi)(\pi\pi\pi)$are fitted with single Gaussian.

$$f_{Sig} = f_1 \mathcal{G}(m|\mu_1\sigma_1) + (1 - f_1)\mathcal{G}(m|\mu_2\sigma_2) \tag{5}$$

The Gaussians within one template are constrained to have common mean value. The ratios of their norms and widths are fixed from Monte Carlo. The yield is integrated using *effective width* - the window containing 95.45% of the signal.

The width and mass of the signal are not well described by Monte Carlo. Signal in data is 2 ± 0.5MeV wider. This difference is studied in [1]

$B^0 \to D_s^+ D^-$ modes have only a few hundred events. Fit values, if left free, fluctuate significantly due to the low statistics. To avoid it only norm and mass of the signal templates are left floating for $B^0 \to D_s^+ D^-$ modes. For $B_s \to D_s^+ D_s^-$ modes all parameters but norm of the signal templates are fixed. Fit systematics due to the parameters being fixed is estimated in section 8.1.

5.2 Background Templates $B^0 \to D_s^+ D^-$.

Background fitting function is divided into combinatorial background and physics background. We use the sum of the flat and exponent for the combinatorial background.

$$f_{Comb} = f_1 exp(m|\mu\tau) + f_2 \tag{6}$$

Among physics background several modes required a dedicated study.

- $B^0 \to D_s^{+*} D^-$ modes with lost $\gamma(\pi_0)$ from $D_s^{+*} \to D_s \gamma(\pi^0)$
- $B^0 \to D_s^+ D^{-*}$ modes with lost π_0 from $D^{-*} \to D^- \pi^0$
- $B^0 \to D_s^{+*} D^{-*}$ modes with π^0 and γ or two π^0 lost
- Reflection from semi-generic $B \to D^+ X, D^+ \to K\pi\pi$
- Reflection from $D^+ \to K\pi\pi$ (for modes with $D_s \to K^* K(3\pi)$ only)

Below all the mentioned reflections and templates for them are reviewed in details.

- $B^0 \to D_s^{+*} D^-$ modes with lost $\gamma(\pi_0)$ from $D_s^{+*} \to D_s^+ \gamma(\pi^0)$ create a reflection roughly one pion mass below the signal. It does not have a distinct shape. We fit it with three Gaussians relaying on the excessive statistics of generated Monte Carlo. Featureless $D_s^{+*} \to D_s^+ \gamma$ dominates ($94.2 \pm 2.5\%$) the template. The small double peak due to the admixture of $D_s^{+*} \to D_s^+ \pi^0$ is negligible. Two modes have the same reconstruction efficiency. The systematics due to the uncertainty of D_s^{+*} branching fractions is discussed in section 8.4.

- $B^0 \to D_s^+ D^{-*}$ modes with lost π_0 from $D^{-*} \to D^- \pi^0$ create a double horn structure below the signal mass. In this analysis we are not very concerned about particular shape and origin of physics background as long as it is well reproduced by Monte Carlo. As a side note we may speculate that double-horn structure is the result of $B \to D_s^+ D^{-*}$ decay followed by $D^{-*} \to D^- \pi^0$ where D^{-*} is polarized. As a result, the angle between the π^0 and the D^{-*} momentum follows $cos^2(\theta)$ law. Most of the time, pion will be released either in the direction of D^{-*} momentum, or in the opposite direction. At the same time D^- tends to continue collinear to D^{-*}. Depending on whether the pion was released forward or backward with respect to the D^{-*} momentum, the reconstructed B^0 mass ends up in one of the two horns. We fit the shape with three Gaussians.

- $B^0 \to D_s^{+*} D^{-*}$ modes with lost π^0 and γ or two π^0 create a wide bump shifted from signal by about twice the pion mass. The reflection does not have a distinct shape and fitted with three Gaussians.

- When the signal and the reflections discussed above are removed the rest of semi-generic $D^+ \to K\pi\pi$ is concentrated in the low mass region and could be approximated with the straight line.

- A noticable contribution from $D_s \to f_0\pi, f_0 \to KK$ (table 15) was found by [13] based on Dialitz analysis of 701 D_s decays. We fit it with the simple Gaussian and correct the width by $2.0 MeV$.

- $B^0 \to \ D_s^+ D^-, D_s^+ \to K^* K$ has a noticeable contribution from $B^0 \to \ D^- 3\pi$ where two pions are reconstructed as kaons. The reflection is very wide and lies well above the signal. The template is added to improve the fit quality and does not affect signal yield.

- $B^0 \to D_s^+ D^-, D_s^+ \to K^* K$ has contribution from non resonant $D_s^+ \to KK\pi$. $B^0 \to \ D_s^+ D^-, D_s^+ \to \phi\pi$is much less affected by this reflection because of the narrow ϕ mass window. The contribution from this mode goes under the signal since its particle content is identical to $K^* K$. We fit it with double Gaussian and correct its width by $2.0 MeV$.

- $B^0 \to \ D_s^+ D^-, D_s^+ \to \pi\pi\pi$ has a contribution from $B^0 \to \ D^- 3\pi$ under the signal. The previous result [1] did not take it into account and the yield for $B^0 \to \ D_s^+ D^-, D_s^+ \to \pi\pi\pi$ was overestimated by $\approx 15\%$.

5.3 Background Templates $B_s \to D_s^+ D_s^-$.

Background fitting function is divided into combinatorial background and physics background. We use the sum of the flat and exponent for the combinatorial background (function 6). Among physics background several modes required a dedicated study.

- $B_s \to \ D_s^+ D_s^-, (\phi\pi)(K^* K)$has a strong reflection from $B^0 \to \ D_s^+ D^-, D_s^+ \to \phi\pi$under the signal.

- $B_s \to \ D_s^+ D_s^-, (\phi\pi)(\pi\pi\pi)$has a reflection from $B_s^0 \to \ D_s^+ 3\pi$ under the signal.

Below all the mentioned reflections and templates for them are reviewed in details.

- $B_s \to \ D_s^+ D_s^-, (\phi\pi)(K^* K)$has a strong reflection from $B^0 \to \ D_s^+ D^-, D_s^+ \to \phi\pi$under the signal. We used our signal Monte Carlo from $B^0 \to \ D_s^+ D^-$branching analysis [1] to create the template and find the normalization for it. The template is shown on figure 28 on the left.

- $B_s \to \ D_s^+ D_s^-, (\phi\pi)(\pi\pi\pi)$has a reflection from $B_s^0 \to \ D_s^+ 3\pi$ under the signal. We used our signal Monte Carlo from D_s^+3Pi branching analysis [2] to create the template and find the normalization for it. The template is shown on figure 28 on the right.

When fit is performed most of the template parameters are fixed. Some template normalizations are left floating, some are fixed to values estimated from our best knowledge. The detailed description of the fitting process is given in section 6

6 General Fit Model

Every fit consist of several templates. The shapes of the templates are fixed and only normalizations are allowed to float. Normalizations of several low-statistics templates are fixed to the values estimated from PDG or scaled from observed modes. The template normalization parameters are summarized in table 7. Entry *"free"* in this table means that the norm for the template is floating (the rest of the template parameters are fixed).

All the mass fits have similar combinatorial background which is fitted with a linear combination of flat and exponent (function 6). All 3 parameters of this function are allowed to float: normalization together with the slope for the exponent and normalization for the flat function.

6.1 Features of $B^0 \to D_s^+ D^-$Fit Models (All D_s Channels).

- Signal is fitted with double Gaussian. Only norm and common mass are left floating. The width is fixed to Monte Carlo value corrected by 2.0 ± 0.5 MeV. No mass correction is required because the masses of two D-mesons are constrained to their PDG values during the reconstruction.

- For every mode we made three separate templates: $B \to D_s^{*+} D^-$, $B \to D_s^+ D^{*-}$ and $B \to D_s^{*+} D^{*-}$. Only overall normalization of every template is allowed to float. We did such a thorough study of $B \to D_s^{-*} D^{+*}$ reflections with the perspective to implement it for $B_s \to D_s D_s$ analysis, where extracting $D_s^{(*)} D_s^{(*)}$ yields will add statistics to $\Delta\Gamma$ measurement.

- The rest of semi-generic $B \to D^+ X, D^+ \to K\pi\pi$ background is fitted with the straight line. The turn-on point is fixed and the normalization is left floating.

- $B^0 \to D_s^+ D^-, D_s^+ \to \phi\pi$ reconstructed mass distributions has contribution from $D_s \to f_0\pi$. We generated a realistic Monte Carlo with the correct ratio between $D_s \to \phi\pi, \phi \to KK$ and $D_s \to f_0\pi, f_0 \to KK$ (table 1). We used $B^0 \to D_s^+ D^-, D_s^+ \to \phi\pi$ signal from data to calculate the scaling factor for our Monte Carlo. This factor was used to scale norm of $D_s \to f_0\pi$ template to data yield. The norm of the template is fixed to $(3.5 \pm 2)\%$ of the signal in the final fit. The error is coming from the uncertainty on the branching fraction of $D_s \to f_0\pi, f_0 \to KK$ measured by [13].

- $B^0 \to D_s^+ D^-, D_s^+ \to K^* K$ reconstructed mass distributions has contribution from non-resonant $D_s \to KK\pi$. We generated a realistic Monte Carlo with the correct ratio between $D_s \to \phi\pi, \phi \to KK$ and non-resonant $D_s \to KK\pi$ (table 1). We used $B^0 \to D_s^+ D^-, D_s^+ \to \phi\pi$ signal from data to calculate the scaling factor for our Monte

Carlo. This factor was used to scale norm of non-resonant $D_s \to KK\pi$ template to data yield. The norm of the template is fixed to $(9 \pm 4)\%$ of the signal in the final fit. The error is coming from the uncertainty on the branching fraction of $D_s \to KK\pi$ measured by [13].

- $B^0 \to D_s^+ D^-, D_s^+ \to K^* K$ and $B^0 \to D_s^+ D^-, D_s^+ \to \pi\pi\pi$ both have reflection of $B^0 \to D^- 3\pi$. We used our signal Monte Carlo for $B^0 \to D^- 3\pi$ [2] to make the templates. We used $B^0 \to D^- 3\pi$ signal from data to calculate the scaling factor for Monte Carlo. This factor was used to scale the norm of the templates to data yields. The norms of these two templates are fixed to 30 ± 3 events.

6.2 Features of $B_s \to D_s^+ D_s^-$ Fit Models.

- Signal for $B_s \to D_s^+ D_s^-, (\phi\pi)(K^* K)$is fitted with double Gaussian. The other two signals are fitted with single Gaussian. Only norm of the signal is left floating. The width is fixed to Monte Carlo value corrected by 2.0 ± 0.5 MeV. No mass correction is required because the masses of two D-mesons are constrained to their PDG values during the reconstruction.

- For $B_s \to D_s^+ D_s^-, (\phi\pi)(\phi\pi)$we made templates fot $B_s \to D_s^{*+} D_s^-$ and $B_s \to D_s^{*+} D_s^{*-}$. Only overall normalization of every template is allowed to float ith we wide mass range fit.

- $B_s \to D_s^+ D_s^-, (\phi\pi)(K^* K)$has a strong reflection from $B^0 \to D_s^+ D^-, D_s^+ \to \phi\pi$under the signal. We used our signal Monte Carlo from $B^0 \to D_s^+ D^-$branching analysis [1] to create the template and find the normalization for it. To find the scale factor between data and Monte Carlo we used our $B^0 \to D_s^+ D^-, D_s^+ \to \phi\pi$signal Monte Carlo reconstructed as $B^0 \to D_s^+ D^-, D_s^+ \to \phi\pi$(figure 29 on the left) and real data reconstruction (figure 30 on the left). We apply this scale factor to the overall normalization of the template accuired from the same Monte Carlo reconstructed as $B^0 \to D_s^+ D^-, D_s^+ \to \phi\pi$(figure 28 on the left).

- $B_s \to D_s^+ D_s^-, (\phi\pi)(\pi\pi\pi)$has a reflection from $B_s^0 \to D_s^+ 3\pi$ under the signal. We used our signal Monte Carlo from $B_s^0 \to D_s^+ 3\pi$ branching analysis [2] to create the template and find the normalization for it. To find the scale factor between data and Monte Carlo we used our $B_s^0 \to D_s^+ 3\pi, D_s \to \pi\pi\pi$ signal Monte Carlo reconstructed as $B_s \to D_s^+ D_s^-, (\phi\pi)(\pi\pi\pi)$(figure 29 on the right) and real data reconstruction (figure 30 on the right). We apply this scale factor to the overall normalization of the template accuired from the same Monte Carlo reconstructed as $B_s \to D_s^+ D_s^-, (\phi\pi)(\pi\pi\pi)$(figure 28 on the right).

The final fits for all the modes for `B_CHARM` and `LOWPT` combined are shown on figures 33 - 41.

7 Extraction of Branching Fractions

The results of the data fits for three $B^0 \to D_s^+ D^-$ modes are shown on figures 33 35 and 36. The results of the data fits for three $B_s \to D_s^+ D_s^-$ modes are shown on figures 37 39 and 40. The binned likelihod fits are done in $[5.3, 6.0]$GeV interval. Signal yields for $B^0 \to D_s^+ D^-$ modes with uncertainties are summarized in table 12. Signal yields for $B_s \to D_s^+ D_s^-$ modes with uncertainties are summarized in table 13. Signal template is integrated to include 95.45% of the signal. Branching fractions which were used for calculations are summarized in table 15.

In reconstructed $B_s \to D_s^+ D_s^-$ one of the D_s mesons decays into $\phi\pi$ and the other D_s meson decays into $\phi\pi$, K^*K or $\pi\pi\pi$. In reconstructed $B^0 \to D_s^+ D^-$, D_s meson decays into $\phi\pi$, K^*K or $\pi\pi\pi$. We form $Br(B^0 \to D_s^+ D^-)/Br(B_s \to D_s^+ D_s^-)$ ratios for three diferent D_s modes so that one of the matching D_s branchings cancels out

$$\frac{Br(B_s \to D_s^+ D_s^-, (\phi\pi)(\phi\pi))}{Br(B^0 \to D_s^+ D^-, D_s^+ \to \phi\pi)} \tag{7}$$

$$\frac{Br(B_s \to D_s^+ D_s^-, (\phi\pi)(K^*K))}{Br(B^0 \to D_s^+ D^-, D_s^+ \to K^*K)} \tag{8}$$

$$\frac{Br(B_s \to D_s^+ D_s^-, (\phi\pi)(\pi\pi\pi))}{Br(B^0 \to D_s^+ D^-, D_s^+ \to \pi\pi\pi)} \tag{9}$$

It makes the final answer only depend on $Br(D_s \to \phi\pi)$ and $D^+ \to K\pi\pi$

$$\frac{f_s}{f_d}\frac{Br(B_s \to D_s^+ D_s^-)}{Br(B^0 \to D_s^+ D^-)} = \frac{N(D_s D_s)}{N(D_s D)} \cdot \frac{\epsilon(D_s D)}{\epsilon(D_s D_s)} \cdot \frac{Br(D^+ \to K\pi\pi)}{Br(D_s \to \phi\pi, \phi \to KK)} \tag{10}$$

Here we have to substitute N and ϵ with numbers for $B^0 \to D_s^+ D^-$and $B_s \to D_s^+ D_s^-$ with matching D_s decays.

Using values of efficiencies from tables 9, 11 and yields from tables 12, 13 we calculate the ratio of branching fractions for three different D_s modes separately. For our dataset, we obtain:

$$\frac{f_s}{f_d}\frac{Br(B_s \dot{\to} D_s^+ D_s^-)}{Br(B^0 \to D_s^+ D^-)} = 1.24 \pm 0.44(Stat) \pm 0.29(Br_{\phi\pi}) \tag{11}$$

$$\frac{f_s}{f_d}\frac{Br(B_s \dot{\to} D_s^+ D_s^-)}{Br(B^0 \to D_s^+ D^-)} = 0.57 \pm 0.33(Stat) \pm 0.13(Br_{\phi\pi}) \tag{12}$$

$$\frac{f_s}{f_d}\frac{Br(B_s \dot{\to} D_s^+ D_s^-)}{Br(B^0 \to D_s^+ D^-)} = 1.52 \pm 0.56(Stat) \pm 0.35(Br_{\phi\pi}) \tag{13}$$

Where $(BR_{\phi\pi})$ is the error due to $Br(D^+ \to K\pi\pi)/Br(D_s \to \phi\pi)$. Using the latest PDG value $\frac{f_s}{f_d} = 0.259 \pm 0.038$ we calculate the ratio of branching fractions for three different $B_s \to D_s^+ D_s^-$ modes separately. For our dataset, we obtain:

$$\frac{Br(B_s \to D_s^+ D_s^-)}{Br(B^0 \to \ D_s^+ D^-)} = 4.8 \pm 1.7(Stat) \pm 0.7(f_s/f_d) \pm 1.1(Br_{\phi\pi}) \tag{14}$$

$$\frac{Br(B_s \to D_s^+ D_s^-)}{Br(B^0 \to \ D_s^+ D^-)} = 2.2 \pm 1.3(Stat) \pm 0.3(f_s/f_d) \pm 0.5(Br_{\phi\pi}) \tag{15}$$

$$\frac{Br(B_s \to D_s^+ D_s^-)}{Br(B^0 \to \ D_s^+ D^-)} = 5.9 \pm 2.2(Stat) \pm 0.9(f_s/f_d) \pm 1.4(Br_{\phi\pi}) \tag{16}$$

The error on D_s branching fractions is clearly dominating. The systematic error is not quoted yet. It is discussed in the next section.

8 Systematic Uncertainties

For the moment this analysis is statistically limited with a hope that measurement of D_s branching fractions will be improved soon. Several sources of systematic uncertainty were studied to make sure that systematic error is significantly smaller than statistical error. Several systematics common for all branching fraction analyses were carefully studies in [2].

- The B p_T spectrum. Systematics due to the difference of B-meson spectrum as observed in data comared to Monte Carlo. Systematics of $\pm 3.0\%$ was assigned.

- Systematic due to our limited knowledge of subresonance structure of 3π in $B^0 \to \ D^- 3\pi$ is estimated to be $\pm 2.5\%$.

- The effect of Self-Reflections due to the track swaps is reviewed in [2] and [1]. Double charm reconstruction is much less affected by Self-Reflections. No systematic is assigned.

- B and D lifetimes systematics is studied in [2] To estimate the size of this effect, we varied the B and D meson lifetimes by their world average measurement errors. We then re-weighted the Monte Carlo with respect to $c\tau$ distribution and calculated the corrected efficiency.

The rest of the systematics specific for $B_s \to D_s^+ D_s^-$ is discussed below in details.

8.1 Fit Systematics.

There are several parameters in the fit which are not well defined and affect the signal yield. In this study we address all the known concerns.

- $B_s \to D_s^+ D_s^-$ signal has longer tails compare to $B^0 \to D_s^+ D^-$modes. We take this effect into account by integrating every signal in 95.45% window. No systematics is assigned.

- Due to the small signal yields for $B^0 \to D_s^+ D^-$ modes we have to fix the width of the signal template to the value obtained from Monte Carlo. Study described in section 5.1 shows that the signal in data is 2.0 ± 0.5 MeV wider than Monte Carlo signal. We use the error on this correction to estimate our fit systematics varying signal width by one standard deviation. We also tried to go as far as two standard deviation or fit data with floating width. The results summarized in table 19 show no significant divergense.

- $B^0 \to D_s^+ D^-, D_s^+ \to \phi\pi$mode has $(3.5 \pm 2)\%$ contribution from $D_s \to f_0\pi, f_0 \to KK$ under the signal. The error is due to the poorly known branching fraction. In our Monte Carlo we fix the mass of f_0 to 980 MeV and the width to 50 MeV. The width of this resonance is porly known. Tho estimate systematics we generated Monte Carlo with 100 MeV width for f_0. It changed $D_s \to f_0\pi, f_0 \to KK$ contribution under the signal from 3.5% to 4%. We consider this change negligible compared to the uncertainty due to the branching ratio. To estimate systematics we vary the template within one sigma.

- $B^0 \to D_s^+ D^-, D_s^+ \to K^* K$mode has $(10 \pm 5)\%$ contribution from non-resonant $D_s \to KK\pi$ under the signal. The error is due to the poorly known branching fraction. To estimate systematics we vary the template within one sigma.

- $B^0 \to D_s^+ D^-, D_s^+ \to \pi\pi\pi$ mode has a strong $B^0 \to D^- 3\pi$ reflection under the signal. The size of the reflection is fixed by using the observed number of $B^0 \to D^- 3\pi$. The unknown subresonance content of 3π could be the source of uncertainty because a_1 and $\rho\pi$ components have different reconstruction efficiency. We estimate the uncertainty due to 3π subresonant content the way we did it in [2]. By using Monte Carlo we estimate the reconstruction efficiency for clean $B^0 \to D^+ a_1$ sample and for weighted admixture of $a_1, \rho\pi$ and 3π in the final state. The difference in yield for two samples is found to be less than 20%. We than vary the norm of the $B^0 \to D^- 3\pi$ reflection by $\pm 20\%$ accounting the discussed uncertainty as fit systematics.

- $B_s \to D_s^+ D_s^-, (\phi\pi)(K^* K)$mode has (14 ± 2) contribution from $B^0 \to D_s^+ D^-, D_s^+ \to \phi\pi$ under the signal. The error is due to the statistics of the data fit (figure 30 on the left). To estimate systematics we vary the template norm within one sigma.

- $B_s \to D_s^+ D_s^-, (\phi\pi)(\pi\pi\pi)$mode has (1 ± 0.2) contribution from $B_s^0 \to D_s^+ 3\pi, D_s \to \pi\pi\pi$ under the signal. The error is due to the statistics of the data fit (figure 30 on the right). To estimate systematics we vary the template norm within one sigma.

The results for fit systematics are summarized in table 19. Several sensitive fit parameters were also varied by $\pm 2\sigma$ to make sure that the uncertainty does not diverge uncontrollably. In the final number for fit uncertainty (table 23) we only use results obtained from $\pm 1\sigma$ variations.

8.2 Cut Optimization Systematics.

Because five L_{xy} dependent cuts were used in this analysis, - optimization procedure showed several stable minimums. We had to choose one of the minimums considered the most optimal. To check the significance of our choice we run the optimization procedure from scratch dropping two $L_{xy}/\sigma(L_{xy})$cuts for D-mesons. As a result several cuts were tighten up (table 21) and the yield went down accordingly (table 10). The lost in the signal yield due to the drop of two cus came out very small. In $B_s \to D_s^+ D_s^-$ optimization we used the reduced list of cuts dropping D-meson $L_{xy}/\sigma(L_{xy})$out. No systematic was assigned to the effect.

8.3 Cut Efficiency Systematics.

The agreement of data and Monte Carlo was tested in [2]. The difference is small but has to be taken into account as a systematic error. We study the change of the ratio of the yields for data and Monte Carlo with respect to cut value. We scale the ratio to 1.00 at the default cut values and look for deviation while scanning cuts one by one within reasonable intervals.

Similar study for $B^0 \to D_s^+ D^-, D_s^+ \to \phi\pi$ is shown on figures 42 and 43. Statistical error is much bigger and all of the deviations are well within the error. There is a minor downtrend visible on five out of seven plots. We are estimating its significance by averaging all the points for each cut. The maximum deviation of 4% is observed in $L_{xy}/\sigma(L_{xy})$. We take it as a systematic error.

$B^0 \to D_s^+ D^-, D_s^+ \to K^* K$ and $B^0 \to D_s^+ D^-, D_s^+ \to \pi\pi\pi$ modes have lower statistic and similar studies are dominated by statistical errors and background fluctuations. We assign the same 4% cut systematic error to these two modes.

$B_s \to D_s^+ D_s^-$ modes have even lower statistic and similar studies are dominated by statistical errors and background fluctuations. We assign the same 4% cut systematic error to these two modes.

8.4 $D_s^{(*)} D^{+(*)}$ systematics.

There are several sourses of systematics for the modes with excited D-mesons.

- Fit systematics is summarized in table 20.
  - The width of narrow double horns for $D_s D^{+*}$ was corrected by 2.0 ± 0.5 MeV. To estimate systematics we vary it within the errors the same way it was done for $B^0 \to D_s^+ D^-$signals.
  - The fit has a cut-off at 4.6 GeV. The systematics of this cut-off is defined by cutting the fit at 4.7 GeV.

– The content of the rest of physics background is hard to define and we estimate its shape by using $B \to D^+X$, $D^+ \to K\pi\pi$ semi-generic Monte Carlo. To estimate the systematics we vary the norm of this background by $\pm 1\sigma$ which is approximately equivalent to $\pm 50\%$ of its norm. Even such a wide variation leads to the systematics which is well below statistical error. When the measurement will get more data the analysis of the background should be improved.

- The fractions of D_s^* decay are deifined within $\pm 2.5\%$ error. We checked that the reconstruction efficiencies for two D_s^* decay modes are the same. We assign $\pm 2.5\%$ systematics to account for D_s^* branching fraction uncertainty.
- For cut systematics we use 4% obtained from $B^0 \to\ D_s^+ D^-$cut systematic study.

8.5 Summary of systematic effects

Sample composition and fit systematics for $B^0 \to\ D_s^+ D^-$are summarized in table 23. The systematics for $D_s^{(*)} D^{+(*)}$ is summarized in table 24. We calculate systematic error separately for each mode.

9 Final Results.

9.1 $B_s \to D_s^+ D_s^-$

We calculate systematic error separately for each mode and add it to our result.

$$\frac{f_s}{f_d}\frac{Br(B_s \overset{\cdot}{\to} D_s^+ D_s^-)}{Br(B^0 \to\ D_s^+ D^-)} = 1.24 \pm 0.44(Stat) \pm 0.09(Syst) \pm 0.29(Br_{\phi\pi}) \tag{17}$$

$$\frac{f_s}{f_d}\frac{Br(B_s \overset{\cdot}{\to} D_s^+ D_s^-)}{Br(B^0 \to\ D_s^+ D^-)} = 0.57 \pm 0.33(Stat) \pm 0.07(Syst) \pm 0.13(Br_{\phi\pi}) \tag{18}$$

$$\frac{f_s}{f_d}\frac{Br(B_s \overset{\cdot}{\to} D_s^+ D_s^-)}{Br(B^0 \to\ D_s^+ D^-)} = 1.52 \pm 0.56(Stat) \pm 0.14(Syst) \pm 0.35(Br_{\phi\pi}) \tag{19}$$

Where $(BR_{\phi\pi})$ is the error due to $Br(D^+ \to K\pi\pi)/Br(D_s \to \phi\pi)$. With the latest PDG value $\frac{f_s}{f_d} = 0.259 \pm 0.038$:

$$\frac{Br(B_s \to D_s^+ D_s^-)}{Br(B^0 \to\ D_s^+ D^-)} = 4.8 \pm 1.7(Stat) \pm 0.4(Syst) \pm 0.7(f_s/f_d) \pm 1.1(Br_{\phi\pi}) \tag{20}$$

$$\frac{Br(B_s \to D_s^+ D_s^-)}{Br(B^0 \to\ D_s^+ D^-)} = 2.2 \pm 1.3(Stat) \pm 0.3(Syst) \pm 0.3(f_s/f_d) \pm 0.5(Br_{\phi\pi}) \tag{21}$$

$$\frac{Br(B_s \to D_s^+ D_s^-)}{Br(B^0 \to \ D_s^+ D^-)} = 5.9 \pm 2.2(Stat) \pm 0.6(Syst) \pm 0.9(f_s/f_d) \pm 1.4(Br_{\phi\pi}) \tag{22}$$

The error on D_s branching fractions dominates the measurement. The error on hadron production as well as good part of the branching and systematic error are correlated.

9.2 Combining Results.

To combine results we weight them by efficiency:

$$\frac{Br(B_s \to D_s^+ D_s^-)}{Br(B^0 \to \ D_s^+ D^-)} = \frac{N_{11} + N_{12} + N_{13}}{N_{01} + N_{02} + N_{03}} \cdot \frac{\epsilon_{01} + r_1 \epsilon_{02} + r_2 \epsilon_{03}}{\epsilon_{11} + r_1 \epsilon_{12} + r_2 \epsilon_{13}} \cdot \frac{Br(D^+ \to K\pi\pi^+)}{Br(D_s^+ \to \phi\pi^+)} \tag{23}$$

Where $r_1 = \frac{\Gamma(K^+ \bar{K}^*(892)^0, \bar{K}_0^* \to K^- \pi^+)}{\Gamma(\phi\pi^+)}$, $r_2 = \frac{\Gamma(\pi\pi\pi)}{\Gamma(\phi\pi^+)}$.

First index 0 is used for $B^0 \to \ D_s^+ D^-$and 1 for $B_s \to D_s^+ D_s^-$. Second indeces 1,2,3 used for decays with $\phi\pi$, $K^* K$ and $\pi\pi\pi$ correspondently.

The first part of the formula with yield ratios provides the total statistical error. The second part with efficiencies gives us a combination of non-correlated branching errors. The third part with $Br(D_s \to \phi\pi)$ is the source of correlated branching error which is the same for all three channels. The part of the systematic uncertainty which is coming from B-meson p_t spectrum and selection cuts (5% total) is considered correlated and is propagated to the final result without change. The systematic uncertainties individual for the channels (fit systematics) are combined weighted statistically by measured yield. Taking everything into account we may write the combined result:

$$\frac{f_s}{f_d} \frac{Br(B_s \dot{\to} D_s^+ D_s^-)}{Br(B^0 \to \ D_s^+ D^-)} = 1.00 \pm 0.24(Stat) \pm 0.06(Syst) \pm 0.04(Br) \pm 0.23(Br_{\phi\pi}) \tag{24}$$

$$\frac{Br(B_s \to D_s^+ D_s^-)}{Br(B^0 \to \ D_s^+ D^-)} = 3.84 \pm 0.93(Stat) \pm 0.24(Syst) \pm 0.56(f_s/f_d) \pm 0.15(Br) \pm 0.89(Br_{\phi\pi}) \tag{25}$$

9.3 $B^0 \to D_s^{(*)} D^{+(*)}$

For $D_s^{(*)} D^{+(*)}$ modes we get.

$$\frac{Br(B^0 \to D_s^* D^+)}{Br(B^0 \to \ D_s^+ D^-)} = 0.89 \pm 0.2 \pm 0.08 \tag{26}$$

$$\frac{Br(B^0 \to D_s D^{+*})}{Br(B^0 \to \ D_s^+ D^-)} = 1.47 \pm 0.4 \pm 0.07 \tag{27}$$

$$\frac{Br(B^0 \to D_s^* D^{+*})}{Br(B^0 \to \ D_s^+ D^-)} = 2.59 \pm 0.5 \pm 0.16 \tag{28}$$

There is no branching fraction error in this measurement since $D_s \to \phi\pi$ and $D^+ \to K\pi\pi$ branching fractions cancel in the ratios.

9.4 Compare to PDG

There is no $B_s \to D_s D_s$ result in PDG to compare. From PDG (2005) we got current best measurements for $B^0 \to \ D_s^{+(*)} D^{-(*)}$:

$$\frac{Br(B^0 \to D_s^* D^+)}{Br(B^0 \to \ D_s^+ D^-)} = 1.25 \pm 0.6 \tag{29}$$

$$\frac{Br(B^0 \to D_s D^{+*})}{Br(B^0 \to \ D_s^+ D^-)} = 1.3 \pm 0.6 \tag{30}$$

$$\frac{Br(B^0 \to D_s^* D^{+*})}{Br(B^0 \to \ D_s^+ D^-)} = 2.4 \pm 1.1 \tag{31}$$

While consistent with PDG our measurements are almost two times better. We are eager to see the first results from Cleo-C for D-meson branching fractions to plug them into our result. We used this analysis as a practice ground for our B_s reconstruction techniques. We plan to continue with $Br(B_s \to D_s D_s)/Br(B^0 \to \ D_s^+ D^-)$.

Acknowledgments

We are grateful to many people who helped us with support, advice and constructive criticism. We would like to thank Gerry Bauer, Stefano Giagu, Rob Harr, Matt Herndon, Rolf Oldeman, for answering many questions that came up in the process. We also would like to note Ricardo Lachman, - our summer student, who helped a lot testing our tools.

References

[1] A. Belloni, A. Bolshov, B. Iyutin, Ch. Paus Title: Measuring the Ratio of Branching Fractions, $Br(B^0 \to \ D_s^+ D^-)/Br(B^0 \to \ D^- 3\pi)$. Draft. CDF note 7925

[2] A. Belloni, A. Bolshov, B. Iyutin, Ch. Paus Measurement of the Ratio of Branching Fractions $Br(B_s^0 \to \ D_s^+ 3\pi)/Br(B^0 \to \ D^- 3\pi)$. CDF note 7815

[3] A. Belloni, I.K. Furić, Ch. Paus, "Study of B_s, B^+ and B^0 Yields in the Hadronic B Samples", CDF Note 6614.

[4] B. Ashmanskas, A. Cerri, see CdfCode browser: http://cdfcodebrowser.fnal.gov/CdfCode/source/svtsim/.

[5] K. Anikeev, P. Murat, Ch. Paus, "Description of Bgenerator II", CDF Note 5092.

[6] P. Nason, S. Dawson and R.K. Ellis, Nucl. Phys. **B303** (1988) 607; Nucl. Phys. **B327** (1989) 49.

[7] C. Peterson *et al.*, Phys. Rev. **D27** (1983) 105.

[8] W. Bell, J.P. Fernandez, L. Flores, F. Wuerthwein, R.J. Tesarek, "User Guide For EvtGen CDF", CDF Note 5618.

[9] A. Cerri, M. Rescigno, "The CDFII Realistic Simulation Package" - CDF Note in preparation.

[10] H.W.Zhao "Study of B Decays into the Final State $D^{(*)}\pi\pi\pi$ at BaBar" hep-ex/0409055

[11] (D. Acosta et al., The CDF Collaboration) "Measurement of $Br(\Lambda_b \to \Lambda_c\pi)/Br(B^0 \to D^+\pi) \cdot \sigma(\Lambda_b)/\sigma(B^0)$" CDF Note 7427

[12] B_s Mixing group "Updated Study of B_s Oscillations in $B_s \to D_s(3)\pi$" CDF Note 7861

[13] (Frabetti et al., FNAL E687 Collab) PL B351 591, Dialitz fit, 701 evts

[14] G Bauer, A Belloni, A Bolshov, B Iyutin, Ch Paus "Measurement of the ratio of Branching fractions $Br(B_s \to D_s\pi)/Br(B_d \to D^+\pi)$ with $355pb^{-1}$" CDF Note 7862

10 Tables

```
Decay anti-B0
0.0080   D+     D_s-                        PHSP;
0.0107   D*+    D_s-                        SVS;
0.0100   D_s*-  D+                          SVS;
0.0190   D_s*- D*+       SVV_HELAMP 0.48 0.0 0.734 0.0 0.48 0.0;
Enddecay
#
Decay D+
0.0900   K-  pi+  pi+                     D_DALITZ;
Enddecay
#
Decay D_s-
0.0228    K*0   K-                        SVS;
0.0180    phi   pi-                       SVS;
0.0090    K+ K- pi-                       PHSP;
0.0004    rho0   pi-                      SVS;
0.0100    f_0    pi-                      PHSP;
0.0020    f_2    pi-                      PHSP;
0.0033    f'_0   pi-                      PHSP;
Enddecay
#
Decay K*0
0.6657      K+  pi-                       VSS;
Enddecay
Decay phi
0.4910   K+   K-                          VSS;
Enddecay
Decay f_0
0.5200   pi+  pi-                         PHSP;
0.4800   K+   K-                          PHSP;
Enddecay
Decay f_2
0.5650   pi+  pi-                         TSS;
Enddecay
Decay f'_0
0.5200   pi+  pi-                         PHSP;
Enddecay
```

Table 1: Decay table for $B^0 \rightarrow \; D_s^{+(*)} D^{-(*)}$

```
Decay B_s0
0.008      D_s-      D_s+               PHSP;
0.010      D_s*+     D_s-               SVS;
0.010      D_s*-     D_s+               SVS;
0.0188     D_s*-     D_s*+              SVV_HELAMP 0.48 0.0 0.734 0.0 0.48 0.0;
Enddecay
#
Decay D_s+
0.0228     anti-K*0  K+                 SVS;
0.0180     phi       pi+                SVS;
0.0090     K+ K- pi+                    PHSP;
0.0004     rho0      pi+                SVS;
0.0100     f_0       pi+                PHSP;
0.0020     f_2       pi+                PHSP;
0.0033     f'_0      pi+                PHSP;
Enddecay
#
Decay K*0
0.6657     K+  pi-                      VSS;
Enddecay
#
Decay phi
0.4910     K+   K-                      VSS;
Enddecay
#
Decay f_0
0.5200     pi+  pi-                     PHSP;
0.4800     K+   K-                      PHSP;
Enddecay
#
Decay f_2
0.5650     pi+  pi-                     TSS;
Enddecay
#
Decay f'_0
0.5200     pi+  pi-                     PHSP;
Enddecay
```

Table 2: Decay table for $B^0 \rightarrow\ D_s^{+(*)} D_s^{-(*)}$

Part	Cut	$B^0 \to D_s D^+(\phi\pi)$	$B^0 \to D_s D^+(K^*K)$	$B^0 \to D_s D^+(\pi\pi\pi)$
B	$\frac{L_{xy}}{\sigma(L_{xy})}$	> 6	> 6	> 4
B	$d0$	< 0.008 cm	< 0.008 cm	< 0.0075 cm
B	$\chi^2_{r\phi}$	< 20	< 17	< 13
D_s	$\frac{L_{xy}}{\sigma(L_{xy})}$	> 5	> 5	> 10
D_s	$L_{xy}^{\leftarrow B}$	> -0.02 cm	> 0.0 cm	> -0.02 cm
D_s	$\chi^2_{r\phi}$	< 15	< 15	< 15
D^+	$\frac{L_{xy}}{\sigma(L_{xy})}$	> 6	> 13	> 12
D^+	$L_{xy}^{\leftarrow B}$	> -0.02 cm	> 0.0 cm	> -0.02 cm
D^+	$\chi^2_{r\phi}$	< 15	< 15	< 15
ϕ	M	$[1.010, 1.029]$		
K^*	M		$[0.84, 0.94]$	
Track	$MinP_T$	$> 0.35 GeV/c$	$> 0.35 GeV/c$	$> 0.35 GeV/c$

Table 3: $B^0 \to D_s^+ D^-, D_s^+ \to \phi\pi$, $B^0 \to D_s^+ D^-, D_s^+ \to K^*K$ and $B^0 \to D_s^+ D^-, D_s^+ \to \pi\pi\pi$ optimized cuts for `B_CHARM` and `LOWPT` combined .

Part	Cut	$B_s \to D_s D_s(\phi\pi)$	$B_s \to D_s D_s(K^*K)$	$B_s \to D_s D_s(\pi\pi\pi)$
B	$\frac{L_{xy}}{\sigma(L_{xy})}$	> 5	> 3.5	> 4
B	$d0$	< 0.012 cm	< 0.006 cm	< 0.007 cm
B	$\chi^2_{r\phi}$	< 16	< 14	< 10
D_s	$L_{xy}^{\leftarrow B}$	> -0.0 cm	> -0.02 cm	> -0.01 cm
D_s	$\chi^2_{r\phi}$	< 15	< 15	< 15
D_s	$L_{xy}^{\leftarrow B}$	> -0.0 cm	> -0.02 cm	> -0.01 cm
D_s	$\chi^2_{r\phi}$	< 15	< 15	< 15
ϕ	M	$[1.010, 1.029]$	$[1.010, 1.029]$	$[1.010, 1.029]$
K^*	M		$[0.84, 0.94]$	
D^+ Veto	M		$[1.845, 1.893]$	
Track	$MinP_T$	$> 0.5 GeV/c$	$> 0.5 GeV/c$	$> 0.5 GeV/c$

Table 4: $B_s \to D_s^+ D_s^-, (\phi\pi)(\phi\pi)$, $B_s \to D_s^+ D_s^-, (\phi\pi)(K^*K)$ and $B_s \to D_s^+ D_s^-, (\phi\pi)(\pi\pi\pi)$ optimized cuts for `B_CHARM` and `LOWPT` combined .

Channel	`B_CHARM`	`B_CHARM` and `LOWPT`	Gain %
$B^0 \to D_s D^+(\phi\pi)$	897 ± 29	1191 ± 34	$33\% \pm 3\%$
$B^0 \to D_s D^+(K^*K)$	614 ± 24	829 ± 28	$35\% \pm 4\%$
$B^0 \to D_s D^+(\pi\pi\pi)$	440 ± 21	566 ± 23	$29\% \pm 5\%$
$B_s \to D_s D_s(\phi\pi)$	156 ± 12	231 ± 14	$48\% \pm 8\%$
$B_s \to D_s D_s(K^*K)$	332 ± 18	434 ± 20	$31\% \pm 5\%$
$B_s \to D_s D_s(\pi\pi\pi)$	153 ± 12	224 ± 14	$46\% \pm 8\%$

Table 5: Gain due to the addition of `LOWPT` triggers. Signal Monte Carlo.

	$B \to D_s D^+$ $D_s \to \phi\pi$	$B \to D_s D^+$ $D_s \to K^*K$	$B \to D_s D^+$ $D_s \to \pi\pi\pi$
$D_s^* D^+$	free	free	free
$D_s D^{+*}$	free	free	free
$D_s^* D^{+*}$	free	free	free
$B^0 \to D^- 3\pi$	-	30 ± 3	30 ± 3
$B \to D^+ X, D^+ \to K\pi\pi$	free	free	free
Combinatorial	free	free	free

Table 6: Templates with fixed normalization.

	$B_s \to D_s D_s$ $(\phi\pi)(\phi\pi)$	$B_s \to D_s D_s$ $(\phi\pi)(K^*K)$	$B_s \to D_s D_s$ $(\phi\pi)(\pi\pi\pi)$
$B^0 \to D_s^+ D^-, D_s^+ \to \phi\pi$	-	10 ± 2	-
$B_s^0 \to D_s^+ 3\pi$	-		1 ± 0.2
$D_s^* D_s$	free	-	-
$D_s^* D_s^*$	free	-	-
$B_s \to D_s X, D_s \to \phi\pi$	free	-	-
Combinatorial	free	free	free

Table 7: Templates with fixed normalization.

Channel	$B^0 \to D_s D^+(\phi\pi)$	$B^0 \to D_s D^+(K^*K)$	$B^0 \to D_s D^+(\pi\pi\pi)$
$B^0 \to D_s D^+(\phi\pi)$	100.0%	$0.4\% \pm 0.2\%$	0.0%
$B^0 \to D_s D^+(K^*K)$	$0.4\% \pm 0.2\%$	100.0%	0.0%
$B^0 \to D_s D^+(\pi\pi\pi)$	$0.0\% \pm 0.1\%$	0.0%	100.0%

Table 8: Cross talk between different $B^0 \to D_s^+ D^-$ channels.

	$B^0 \to D_s D^+(\phi\pi)$	$B \to D_s D^+(K^*K)$	$B^0 \to D_s D^+(\pi\pi\pi)$
Generated ($\times 10^6$)	2.765	3.503	1.675
Yield MC Combined	1191 ± 34	829 ± 28	566 ± 23
Eff Combined ($\times 10^{-3}$)	0.431 ± 0.012	0.237 ± 0.008	0.338 ± 0.014

Table 9: Efficiencies extracted from Monte Carlo for $B^0 \to D_s^+ D^-$.

	$B^0 \to D_s D^+(\phi\pi)$	$B^0 \to D_s^* D^+$	$B^0 \to D_s D^{+*}$	$B^0 \to D_s^* D^{+*}$
Generated ($\times 10^6$)	2.765	4.35	4.66	8.25
Yield MC Combined	1191 ± 34	1724 ± 42	526 ± 23	938 ± 31
Eff Combined ($\times 10^{-3}$)	0.424 ± 0.011	0.396 ± 0.010	0.113 ± 0.005	0.114 ± 0.003

Table 10: Efficiencies extracted from Monte Carlo for $B^0 \to D_s^{+(*)} D^{-(*)}$.

	$B_s \to D_s D_s(\phi\pi)$	$B_s \to D_s D_s(K^*K)$	$B_s \to D_s D_s(\pi\pi\pi)$
Generated ($\times 10^6$)	2.819	3.570	1.707
Yield MC Combined	231 ± 15	434 ± 20	224 ± 13
Eff Combined ($\times 10^{-3}$)	0.082 ± 0.005	0.122 ± 0.006	0.131 ± 0.008

Table 11: Efficiencies extracted from Monte Carlo for $B_s \to D_s^+ D_s^-$.

	$B^0 \to D_s D^+(\phi\pi)$	$B^0 \to D_s D^+(K^*K)$	$B^0 \to D_s D^+(3\pi)$
Yield	185 ± 16	132 ± 14	91 ± 13

Table 12: Yields extracted from Data.

	$B_s \to D_s D_s(\phi\pi)$	$B_s \to D_s D_s(K^*K)$	$B_s \to D_s D_s(3\pi)$
Yield	8.6 ± 2.9	7.6 ± 4.3	10.5 ± 3.5

Table 13: Yields extracted from Data.

	$B^0 \to D_s D^+(\phi\pi)$	$B^0 \to D_s^* D^+$	$B^0 \to D_s D^{+*}$	$B^0 \to D_s^* D^{+*}$
Yield Data Combined	185 ± 16	158 ± 34	75 ± 22	133 ± 25

Table 14: Yields extracted from Data $B^0 \to D_s^{+(*)} D^{-(*)}$.

D^+ Decays	Branching
$\Gamma(K^-\pi^+\pi^+)/\Gamma_{total}$	0.092 ± 0.006
D_s Decays	Branching
$\Gamma(D_s \to K^+K^-\pi^+)/\Gamma_{total}$	0.043 ± 0.012
$\Gamma(\phi\pi^+, \phi \to K^+K^-)/\Gamma_{total}$	0.018 ± 0.004
$\Gamma(K^+\bar{K}^*(892)^0, \bar{K}^*(892)^0 \to K^-\pi^+)/\Gamma_{total}$	0.020 ± 0.006
$\Gamma(\pi^+\pi^+\pi^-)/\Gamma_{total}$	0.0101 ± 0.003
$\Gamma(K^+K^-\pi^+NR)/\Gamma_{total}$	0.009 ± 0.004
$\Gamma(f_0(980)\pi^+, f_0 \to K^+K^-)/\Gamma(K^+K^-\pi^+)$	$0.11 \pm 0.035 \pm 0.026$
$\Gamma(K^+\bar{K}_0^*(1430)^0, \bar{K}_0^* \to K^-\pi^+)/\Gamma(K^+K^-\pi^+)$	$0.093 \pm 0.032 \pm 0.032$
$\Gamma(K^+\bar{K}^*(892)^0, \bar{K}^*(892)^0 \to K^-\pi^+/\Gamma(\phi\pi^+, \phi \to K^+K^-)$	1.25 ± 0.12
$\Gamma(\pi^+\pi^+\pi^-)/\Gamma(\phi\pi^+, \phi \to K^+K^-)$	0.565 ± 0.071

Table 15: Relevant branching fractions and ratios of branching fractions with uncertainties.

Meson	Lifetime
B_s	1.461 ± 0.057 ps
B^0	1.536 ± 0.014 ps
D_s^+	490 ± 9 fs
D^+	1040 ± 7 fs

Table 16: B and D meson lifetimes and errors used to estimate systematic effects by rescaling the Monte Carlo

Effect	Syst. Uncertainty [%]
B_s lifetime	$\pm 2.0\%$
D_s^+ lifetime	$\pm 0.0\%$
B^0 lifetime	$\pm 0.4\%$
D^+ lifetime	$\pm 0.0\%$

Table 17: Table of systematic uncertainties due to uncertainties on meson lifetimes

Varied Parameter	Variation	Min	Max	Diff
$B^0 \to D_s D^+(\phi\pi)$		185 ± 16	185 ± 16	
Width	$\pm 1\sigma$	182 ± 16	188 ± 16	$\pm 1.6\%$
Width	$\pm 2\sigma$	179 ± 16	191 ± 16	$\pm 3.2\%$
Width Free		180 ± 16	180 ± 16	$\pm 2.7\%$
Mass Free		186 ± 16	186 ± 16	$\pm 0.6\%$
$D_s \to f_0\pi$	$\pm 1\sigma$	188 ± 16	181 ± 16	$\pm 2.0\%$
$B^0 \to D_s D^+(K^*K)$		132 ± 14	132 ± 14	
Width	$\pm 1\sigma$	130 ± 14	134 ± 14	$\pm 1.5\%$
Width	$\pm 2\sigma$	128 ± 13	136 ± 14	$\pm 3.0\%$
Width Free		136 ± 14	136 ± 14	$\pm 3.0\%$
$D_s \to KK\pi$	$\pm 1\sigma$	137 ± 14	127 ± 14	$\pm 3.5\%$
$B^0 \to D_s D^+(3\pi)$		91 ± 13	91 ± 13	
Width	$\pm 1\sigma$	89 ± 13	93 ± 13	$\pm 2.2\%$
Width	$\pm 2\sigma$	86 ± 12	95 ± 14	$\pm 4.4\%$
Width Free		98 ± 18	98 ± 18	$\pm 7.7\%$
$B \to D^+ 3\pi$	$\pm 20\%$	88 ± 13	94 ± 13	$\pm 3.3\%$

Table 18: Fit systematic errors. Vary the most sensitive parameters.

Varied Parameter	Variation	Min	Max	Diff
$B_s \to D_s D_s(\phi\pi)$		8.6 ± 2.9	8.6 ± 2.9	
Width Free		-	-	$\pm 3.0\%$
Mass Free		-	-	$\pm 0.6\%$
$B_s \to D_s D_s(K^* K)$		7.6 ± 4.3	7.6 ± 4.3	
Width Free		-	-	$\pm 3.0\%$
Mass Free		-	-	$\pm 0.6\%$
$B^0 \to D_s^+ D^-, D_s^+ \to \phi\pi$	$\pm 10\%$	7.1 ± 4.2	8.2 ± 4.3	$\pm 8\%$
$B_s \to D_s D_s(3\pi)$		10.5 ± 3.5	10.5 ± 3.5	
Width Free		-	-	$\pm 3.0\%$
Mass Free		-	-	$\pm 0.6\%$
$B_s \to D_s 3\pi$	$\pm 25\%$	10.4 ± 3.5	10.7 ± 1	$\pm 3.0\%$

Table 19: Fit systematic errors. Vary the most sensitive parameters.

Varied Parameter	Variation	$B^0 \to D_s^* D^+$	$B^0 \to D_s D^{+*}$	$B^0 \to D_s^* D^{+*}$
$B^0 \to D_s D^{+*}$				
Width	$\pm 1\sigma$	$\pm 1.\%$	$\pm 2.0\%$	$\pm 1.0\%$
Width	$\pm 2\sigma$	$\pm 2.\%$	$\pm 4.0\%$	$\pm 1.0\%$
$B^0 \to D^+ X$				
Norm	$\pm 1\sigma$	$\pm 8.\%$	$\pm 2.0\%$	$\pm 1.0\%$
Norm	$\pm 2\sigma$	$\pm 16.\%$	$\pm 4.0\%$	$\pm 2.0\%$
Fit Range	$[4.7, 6.5]$	$\pm 1.\%$	$\pm 0.0\%$	$\pm 4.0\%$

Table 20: Fit systematic errors for $D_s^{(*)} D^{+(*)}$ modes.

Part	Cut	$B^0 \to D_s D^+$, $D_s \to \phi\pi$ Default	$B^0 \to D_s D^+$, $D_s \to \phi\pi$ D $L_{xy}/\sigma(L_{xy})$Dropped
B	$\frac{L_{xy}}{\sigma(L_{xy})}$	> 6	> 6
B	$d0$	< 0.008 cm	< 0.008 cm
B	$\chi^2_{r\phi}$	< 20	< 18
D_s	$\frac{L_{xy}}{\sigma(L_{xy})}$	> 5	Dropped
D_s	$L_{xy}^{\leftarrow B}$	> -0.02 cm	> -0.01 cm
D_s	$\chi^2_{r\phi}$	< 15	< 15
D^+	$\frac{L_{xy}}{\sigma(L_{xy})}$	> 6	Dropped
D^+	$L_{xy}^{\leftarrow B}$	> -0.02 cm	> -0.01 cm
D^+	$\chi^2_{r\phi}$	< 15	< 15
ϕ	M	$[1.010, 1.029]$	$[1.010, 1.029]$
Track	$MinP_T$	$> 0.35 GeV/c$	$> 0.35 GeV/c$

Table 21: Optimization results with D-meson $L_{xy}/\sigma(L_{xy})$cuts droopped.

Channel	Default	Dropped	Change %
$B^0 \to D_s^+ D^-, D_s^+ \to \phi\pi$ Data	185 ± 16	188 ± 15	$-1.5\% \pm 8.0\%$
$B^0 \to D_s^+ D^-, D_s^+ \to \phi\pi$ MC	8470 ± 90	8185 ± 88	$-3.4\% \pm 1.0\%$

Table 22: The change in data and Monte-Carlo yield with D-meson $L_{xy}/\sigma(L_{xy})$cuts droopped from the optimization.

Effect	Syst. Uncertainty [%]
BP_T spectrum	$\pm 3.0\%$
$D_s \to \pi\pi\pi$ composition	$\pm 3.0\%$
$B^0 \to D_s D^+(\phi\pi)$ Fit	$\pm 2.6\%$
$B^0 \to D_s D^+(K^* K)$ Fit	$\pm 4.0\%$
$B^0 \to D_s D^+(\pi\pi\pi)$ Fit	$\pm 4.0\%$
$B_s \to D_s^- D_s^+(\phi\pi)$ Fit	$\pm 3.1\%$
$B_s \to D_s^- D_s^+(K^* K)$ Fit	$\pm 8.5\%$
$B_s \to D_s^- D_s^+(\pi\pi\pi)$ Fit	$\pm 4.5\%$
$B^0 \to D_s^- D^+(\phi\pi)$ Cuts	$\pm 4.0\%$
$B_s \to D_s^- D_s^+(\phi\pi)$ Cuts	$\pm 4.0\%$
Common	$\pm 5.0\%$

Table 23: Table of systematic errors.

Varied Parameter	$B^0 \to D_s^* D^+$	$B^0 \to D_s D^{+*}$	$B^0 \to D_s^* D^{+*}$
Fit Syst	$\pm 8.0\%$	$\pm 3.0\%$	$\pm 4.0\%$
D_s^* Composition	$\pm 2.5\%$		$\pm 2.5\%$
Cut Syst	$\pm 4.0\%$	$\pm 4.0\%$	$\pm 4.0\%$

Table 24: Table of systematic errors for $B^0 \to \ D_s^{+(*)} D^{-(*)}$ modes.

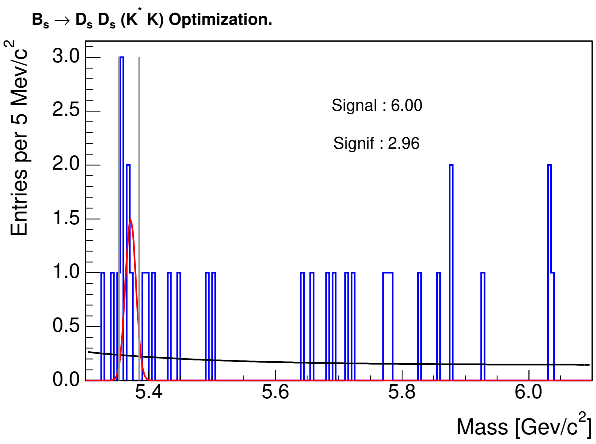

Figure 1: Fitting the signal and background during optimization. Plot shows a snapshot of the optimization process for L_{xy} significance of the B. Grey lines show the region used to calculate signal significance.

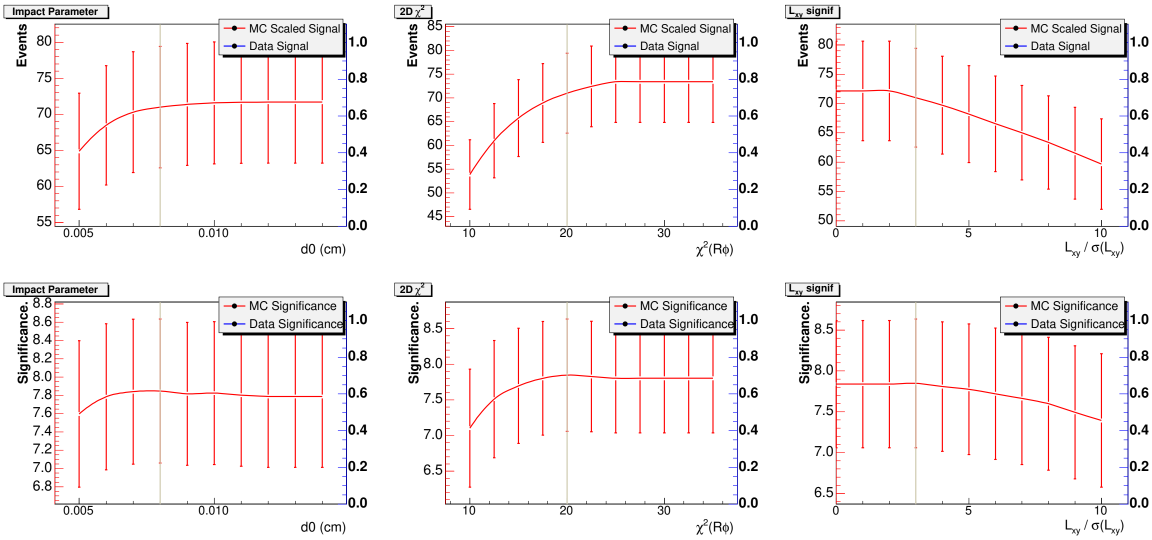

Figure 2: Cut optimization plots for $B^0 \to D_s^+ D^-, D_s^+ \to \phi\pi$: L_{xy} significance of the B, impact parameter of the B, and 2D χ^2 of the$B$ for B_CHARM and LOWPT combined Top plots show number of Monte Carlo scaled signal events, bottom plots - significance $\sigma = S/\sqrt{S+B}$ of the scaled Monte Carlo signal.

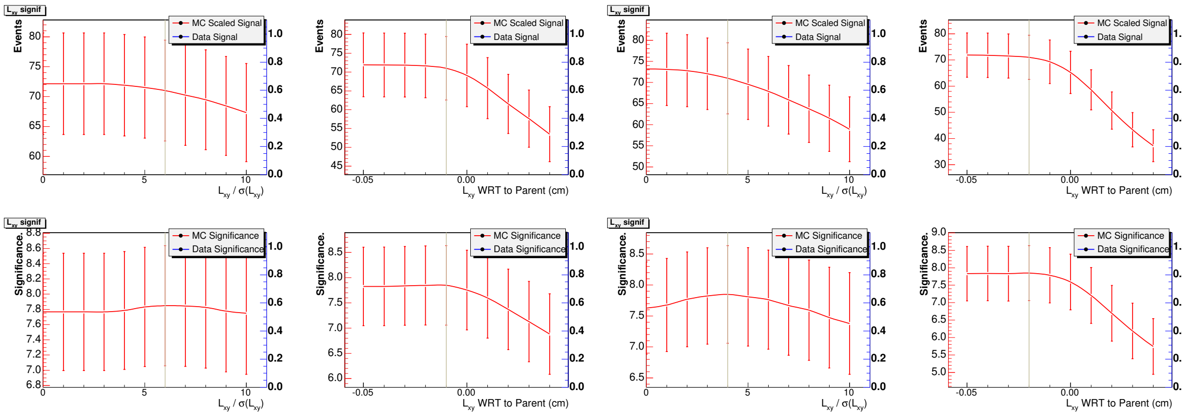

Figure 3: Cut optimization plots for $B^0 \to D_s^+ D^-, D_s^+ \to \phi\pi$: L_{xy} significance of the D^+, L_{xy} of the D^+ with respect to B, L_{xy} significance of the D_s, L_{xy} of the D_s with respect to B. Top plots show number of Monte Carlo scaled signal events, bottom plots - significance $\sigma = S/\sqrt{S+B}$ of the scaled Monte Carlo signal.

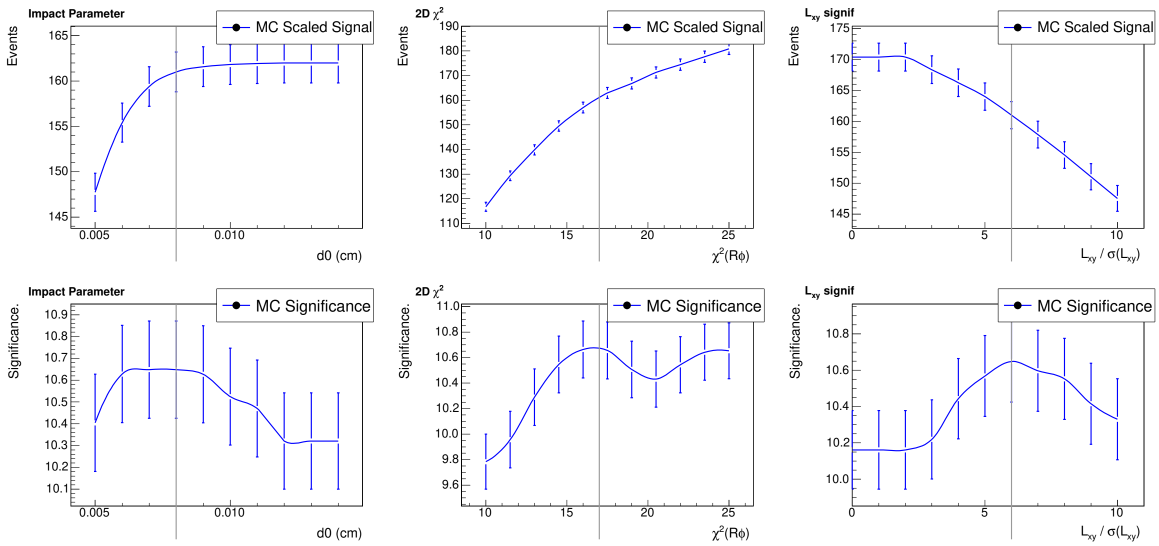

Figure 4: Cut optimization plots for $B^0 \rightarrow \ D_s^+ D^-, D_s^+ \rightarrow K^* K$: L_{xy} significance of the B, impact parameter of the B, and 2D χ^2 of the$B$ for B_CHARM and LOWPT combined Top plots show number of Monte Carlo scaled signal events, bottom plots - significance $\sigma = S/\sqrt{S+B}$ of the scaled Monte Carlo signal.

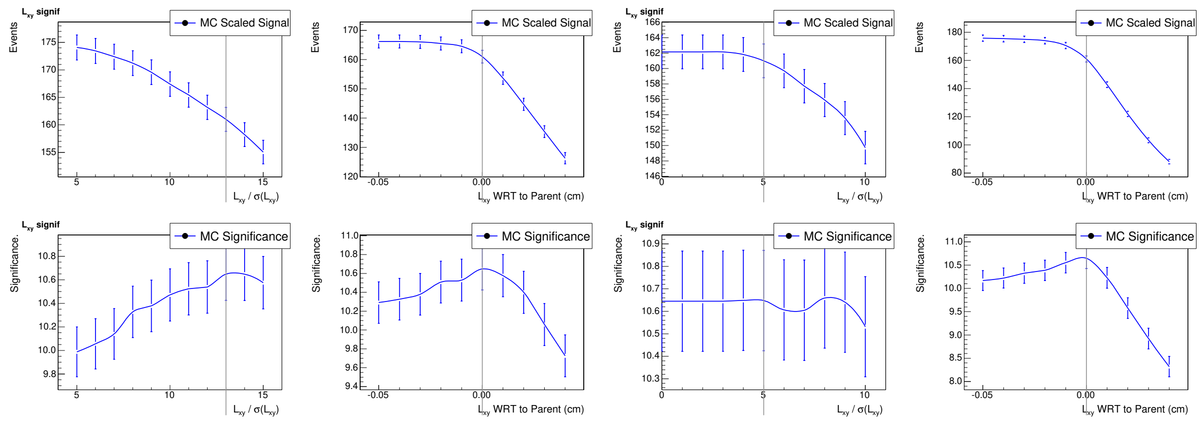

Figure 5: Cut optimization plots for $B^0 \rightarrow \ D_s^+ D^-, D_s^+ \rightarrow K^* K$: L_{xy} significance of the D^+, L_{xy} of the D^+ with respect to B, L_{xy} significance of the D_s, L_{xy} of the D_s with respect to B. Top plots show number of Monte Carlo scaled signal events, bottom plots - significance $\sigma = S/\sqrt{S+B}$ of the scaled Monte Carlo signal.

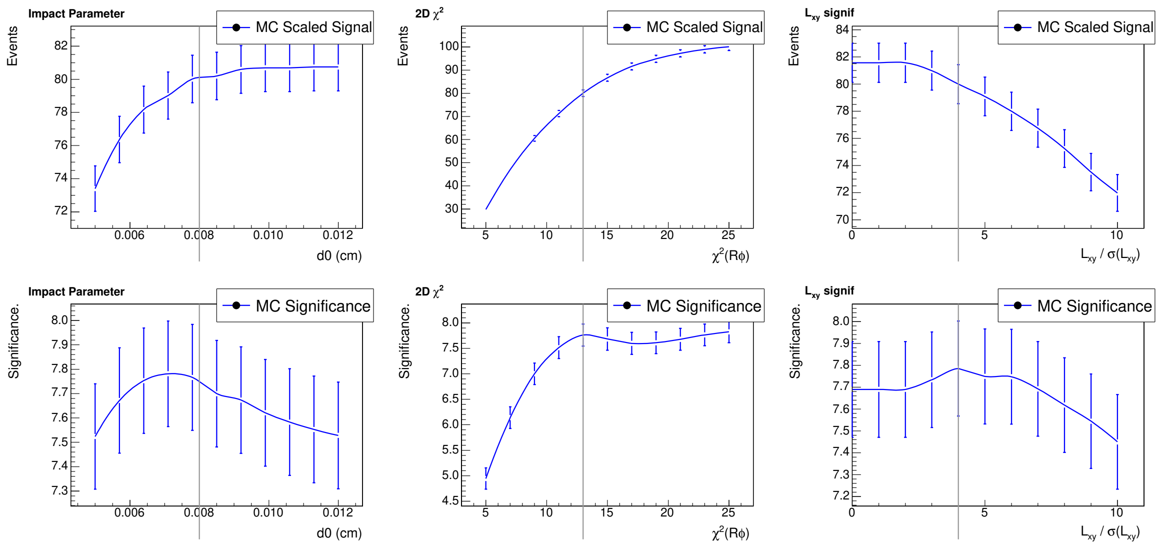

Figure 6: Cut optimization plots for $B^0 \rightarrow D_s^+ D^-, D_s^+ \rightarrow \pi\pi\pi$: L_{xy} significance of the B, impact parameter of the B, and 2D χ^2 of the$B$ for B_CHARM and LOWPT combined Top plots show number of Monte Carlo scaled signal events, bottom plots - significance $\sigma = S/\sqrt{S+B}$ of the scaled Monte Carlo signal.

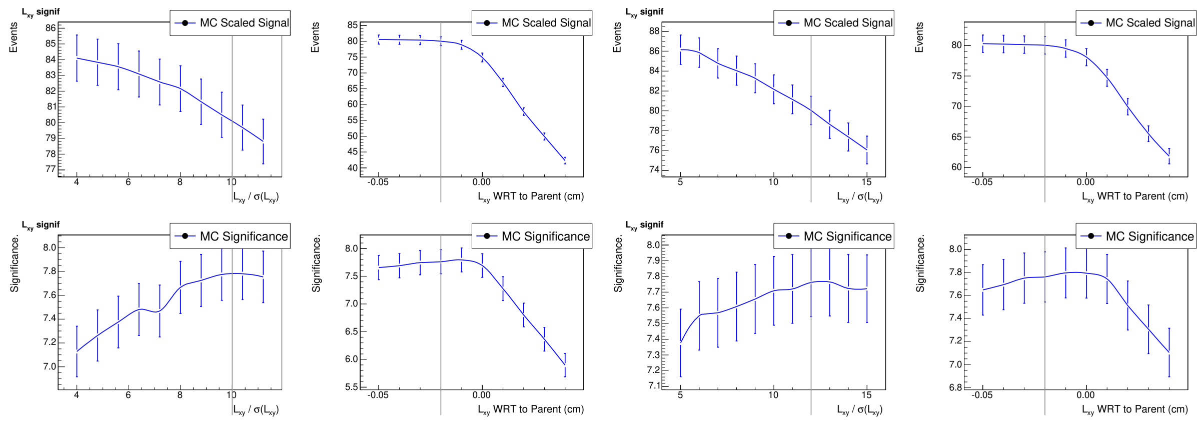

Figure 7: Cut optimization plots for $B^0 \rightarrow D_s^+ D^-, D_s^+ \rightarrow \pi\pi\pi$: L_{xy} significance of the D^+, L_{xy} of the D^+ with respect to B, L_{xy} significance of the D_s, L_{xy} of the D_s with respect to B. Top plots show number of Monte Carlo scaled signal events, bottom plots - significance $\sigma = S/\sqrt{S+B}$ of the scaled Monte Carlo signal.

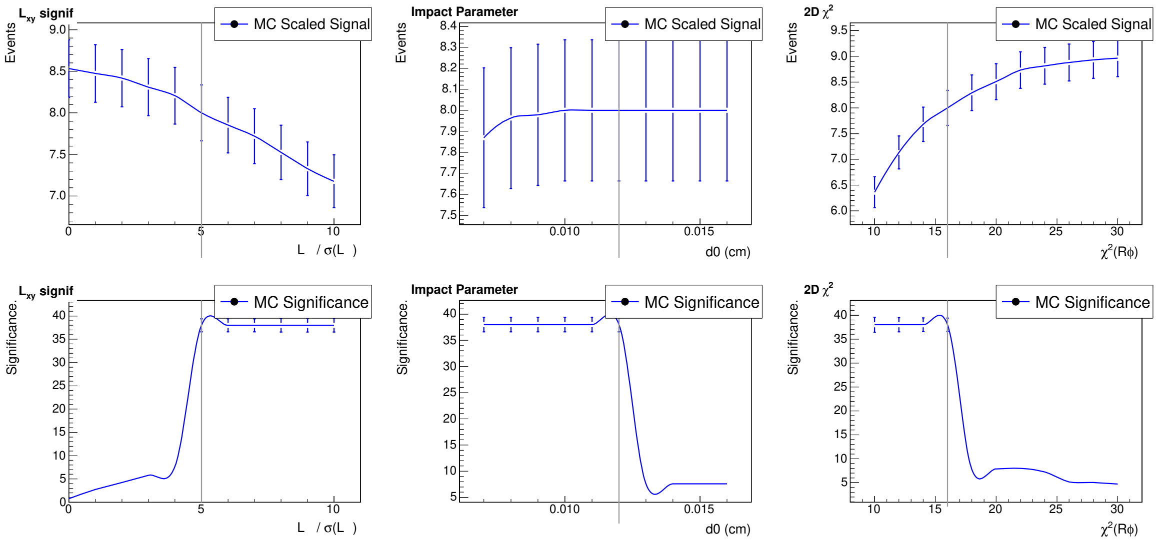

Figure 8: Cut optimization plots for $B_s \to \ D_s^+ D_s^-, (\phi\pi)(\phi\pi)$: L_{xy} significance of the B, impact parameter of the B, and 2D χ^2 of the$B$ for `B_CHARM` and `LOWPT` combined Top plots show number of Monte Carlo scaled signal events, bottom plots - significance $\sigma = S/\sqrt{S+B}$ of the scaled Monte Carlo signal.

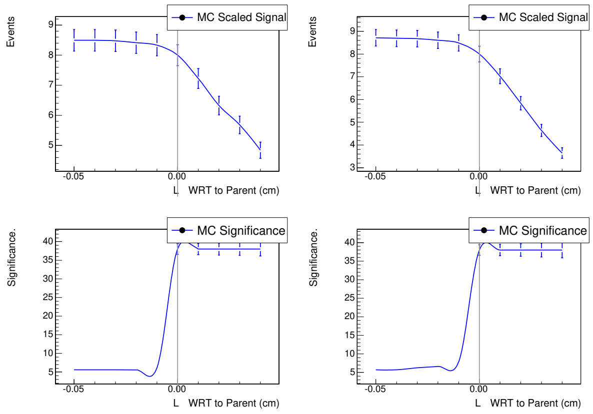

Figure 9: Cut optimization plots for $B_s \to \ D_s^+ D_s^-, (\phi\pi)(\phi\pi)$: L_{xy} of the first D_s with respect to B, L_{xy} of the second D_s with respect to B. Top plots show number of Monte Carlo scaled signal events, bottom plots - significance $\sigma = S/\sqrt{S+B}$ of the scaled Monte Carlo signal.

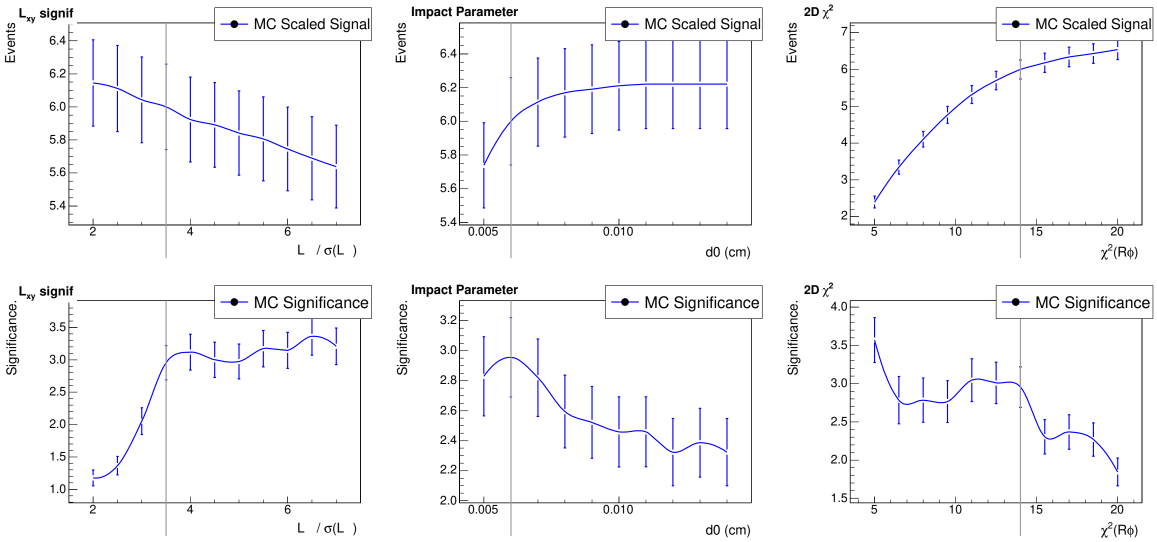

Figure 10: Cut optimization plots for $B_s \rightarrow\ D_s^+ D_s^-, (\phi\pi)(K^*K)$: L_{xy} significance of the B, impact parameter of the B, and 2D χ^2 of the$B$ for `B_CHARM` and `LOWPT` combined Top plots show number of Monte Carlo scaled signal events, bottom plots - significance $\sigma = S/\sqrt{S+B}$ of the scaled Monte Carlo signal.

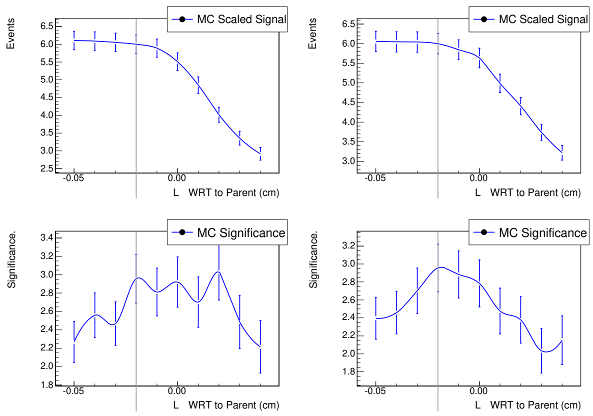

Figure 11: Cut optimization plots for $B_s \rightarrow\ D_s^+ D_s^-, (\phi\pi)(K^*K)$: L_{xy} of the first D_s with respect to B, L_{xy} of the second D_s with respect to B. Top plots show number of Monte Carlo scaled signal events, bottom plots - significance $\sigma = S/\sqrt{S+B}$ of the scaled Monte Carlo signal.

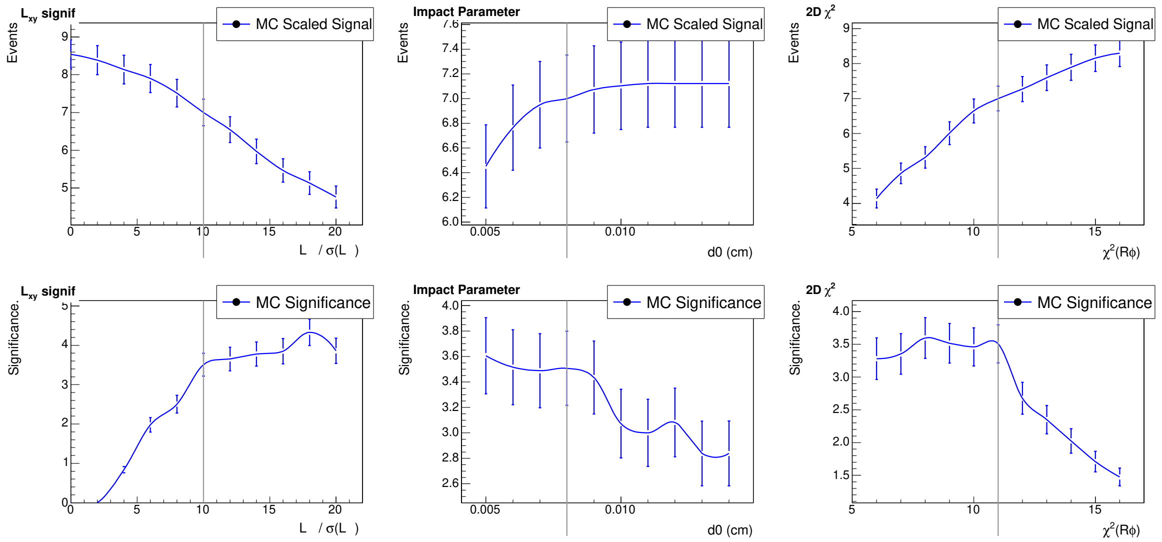

Figure 12: Cut optimization plots for $B_s \rightarrow D_s^+ D_s^-, (\phi\pi)(\pi\pi\pi)$: L_{xy} significance of the B, impact parameter of the B, and 2D χ^2 of the$B$ for `B_CHARM` and `LOWPT` combined Top plots show number of Monte Carlo scaled signal events, bottom plots - significance $\sigma = S/\sqrt{S+B}$ of the scaled Monte Carlo signal.

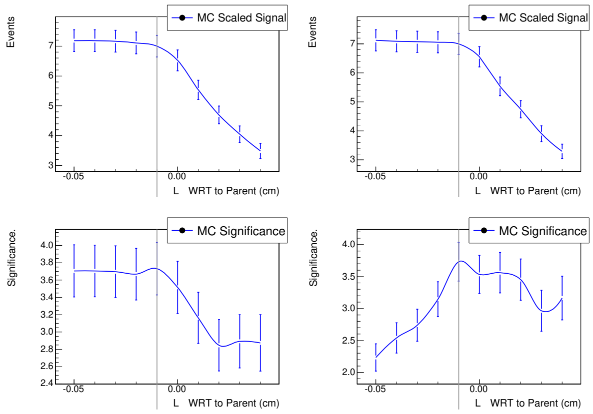

Figure 13: Cut optimization plots for $B_s \rightarrow D_s^+ D_s^-, (\phi\pi)(\pi\pi\pi)$: L_{xy} of the first D_s with respect to B, L_{xy} of the second D_s with respect to B. Top plots show number of Monte Carlo scaled signal events, bottom plots - significance $\sigma = S/\sqrt{S+B}$ of the scaled Monte Carlo signal.

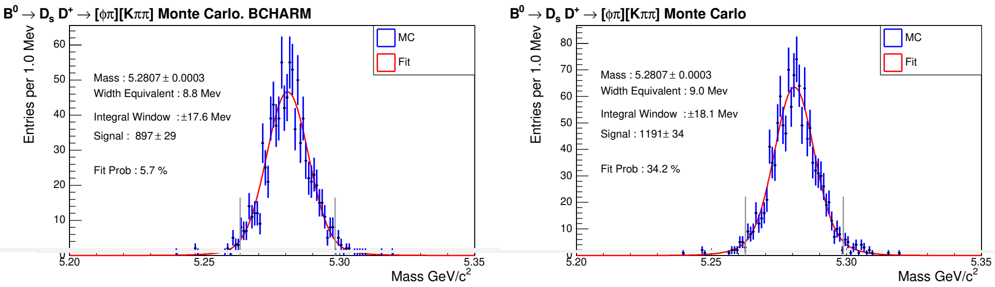

Figure 14: Signal Monte Carlo $B^0 \to D_s^+ D^-, D_s^+ \to \phi\pi$. `B_CHARM` on the left, `B_CHARM` and `LOWPT` combined on the right. Used to extract template parameters and for efficiency studies.

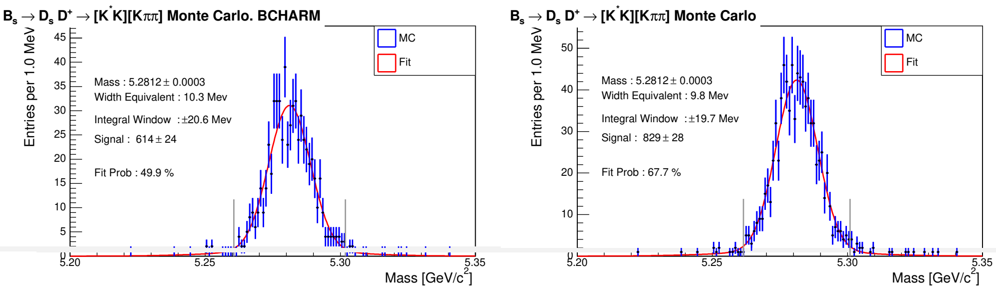

Figure 15: Signal Monte Carlo $B^0 \to D_s^+ D^-, D_s^+ \to K^* K$. `B_CHARM` on the left, `B_CHARM` and `LOWPT` combined on the right. Used to extract template parameters and for efficiency studies.

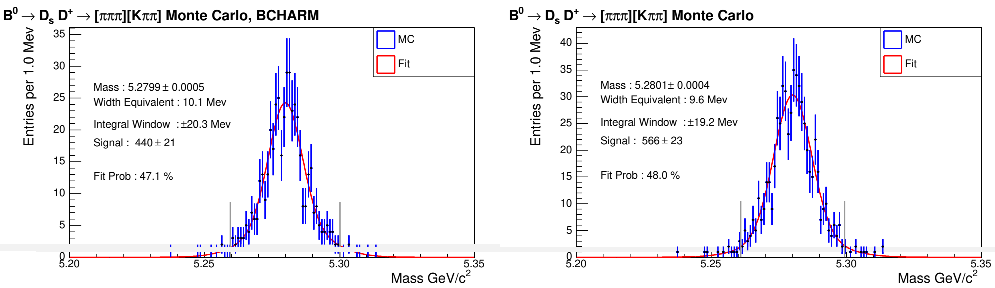

Figure 16: Signal Monte Carlo $B^0 \to D_s^+ D^-, D_s^+ \to \pi\pi\pi$. `B_CHARM` on the left, `B_CHARM` and `LOWPT` combined on the right. Used to extract template parameters and for efficiency studies.

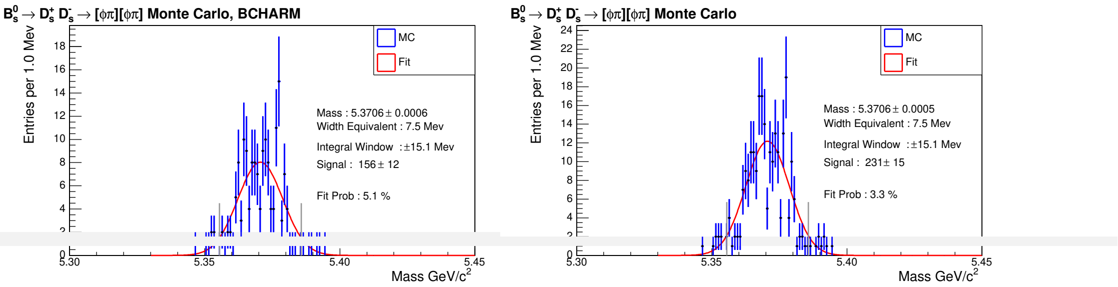

Figure 17: Signal Monte Carlo $B_s \to D_s^+ D_s^-, (\phi\pi)(\phi\pi)$. `B_CHARM` on the left, `B_CHARM` and `LOWPT` combined on the right. Used to extract template parameters and for efficiency studies.

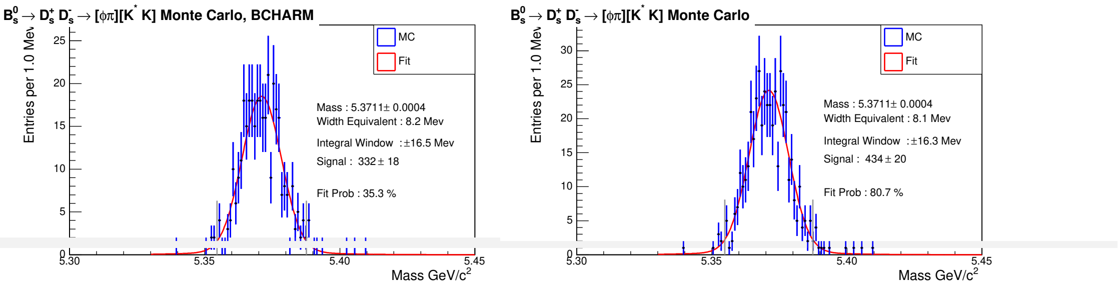

Figure 18: Signal Monte Carlo $B_s \to D_s^+ D_s^-, (\phi\pi)(K^* K)$. `B_CHARM` on the left, `B_CHARM` and `LOWPT` combined on the right. Used to extract template parameters and for efficiency studies.

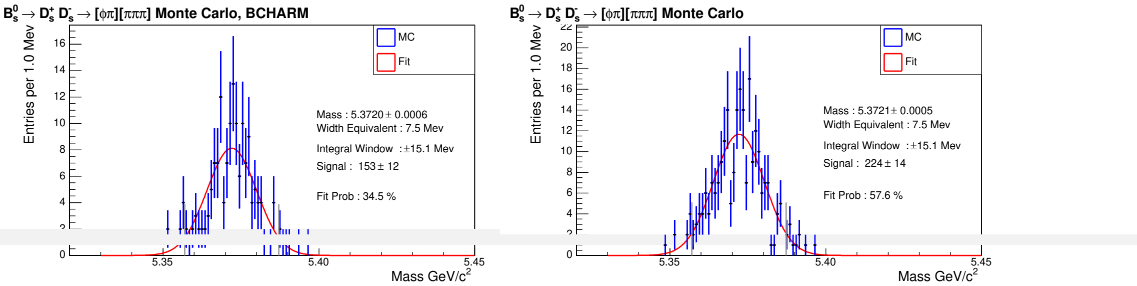

Figure 19: Signal Monte Carlo $B_s \to D_s^+ D_s^-, (\phi\pi)(\pi\pi\pi)$. `B_CHARM` on the left, `B_CHARM` and `LOWPT` combined on the right. Used to extract template parameters and for efficiency studies.

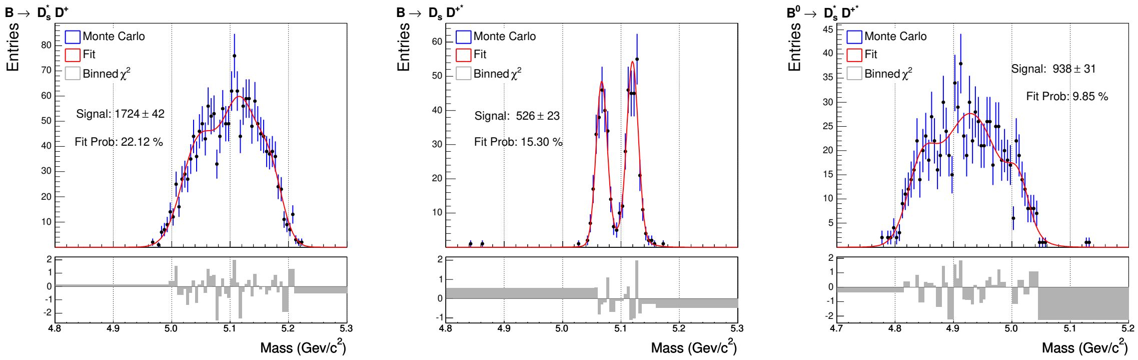

Figure 20: $B^0 \to D_s^{(*)} D^{+(*)}$ templates for $B^0 \to \ D_s^+ D^-, D_s^+ \to \phi\pi$.

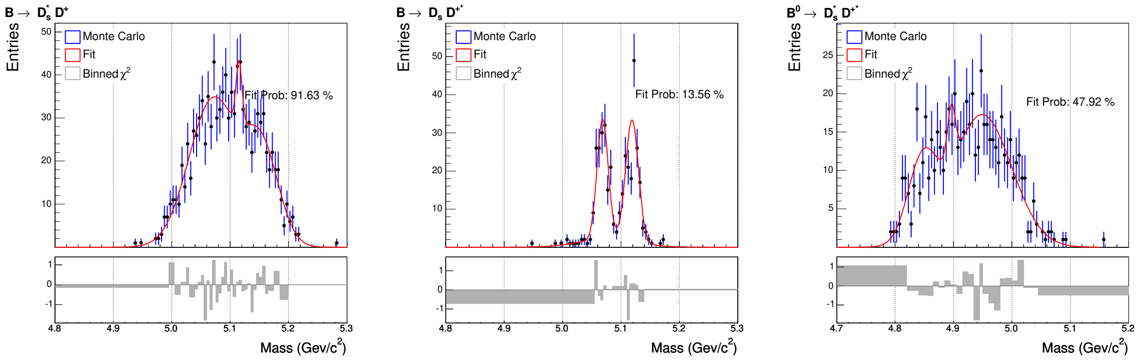

Figure 21: $B^0 \to D_s^{(*)} D^{+(*)}$ templates for $B^0 \to \ D_s^+ D^-, D_s^+ \to K^*K$.

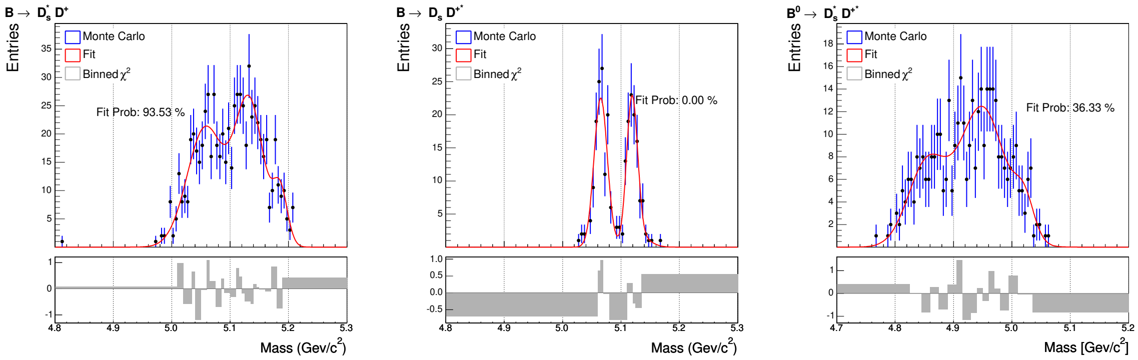

Figure 22: $B^0 \to D_s^{(*)} D^{+(*)}$ templates for $B^0 \to \ D_s^+ D^-, D_s^+ \to \pi\pi\pi$.

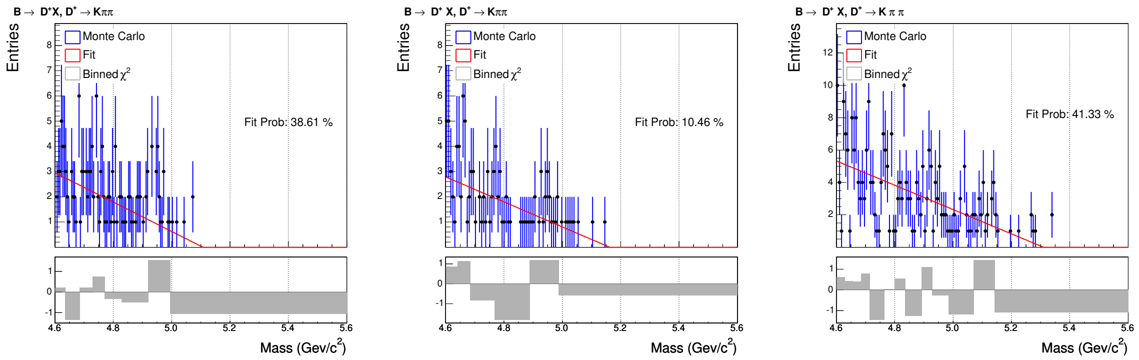

Figure 23: $B^0 \to D_s^{(*)} D^{+(*)}$ templates for $B^0 \to \ D_s^+ D^-, D_s^+ \to \pi\pi\pi$.

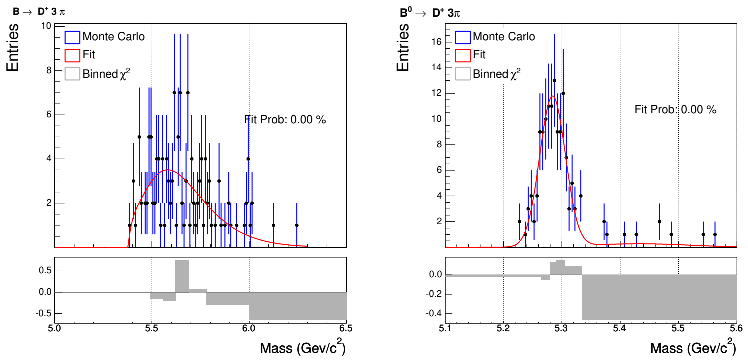

Figure 24: $B^0 \to D_s^{(*)} D^{+(*)}$ templates for $B^0 \to \ D_s^+ D^-, D_s^+ \to \pi\pi\pi$.

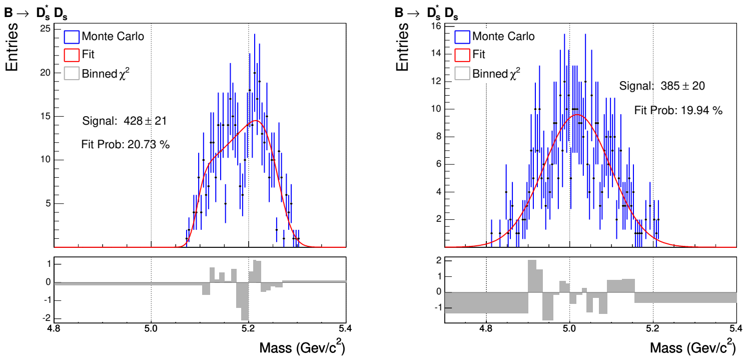

Figure 25: $B^0 \to D_s^{(*)} D^{+(*)}$ templates for $B_s \to \ D_s^+ D_s^-, (\phi\pi)(\phi\pi)$.

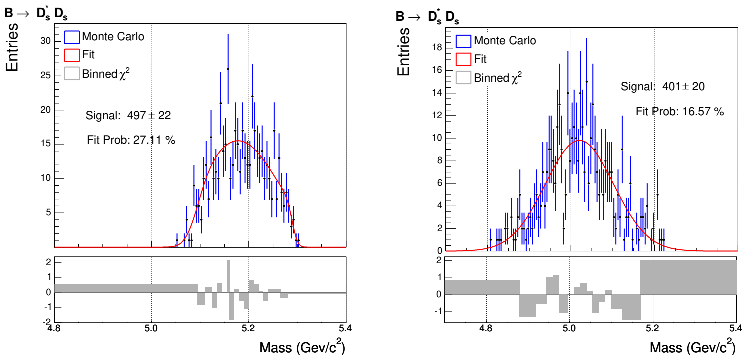

Figure 26: $B^0 \to D_s^{(*)} D^{+(*)}$ templates for $B_s \to \ D_s^+ D_s^-, (\phi\pi)(K^* K)$.

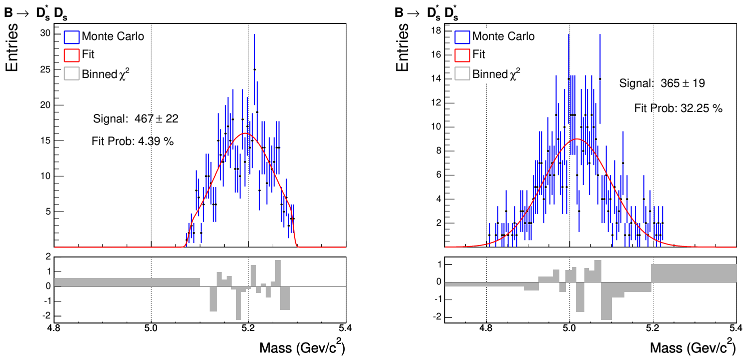

Figure 27: $B^0 \to D_s^{(*)} D^{+(*)}$ templates for $B_s \to \ D_s^+ D_s^-, (\phi\pi)(\pi\pi\pi)$.

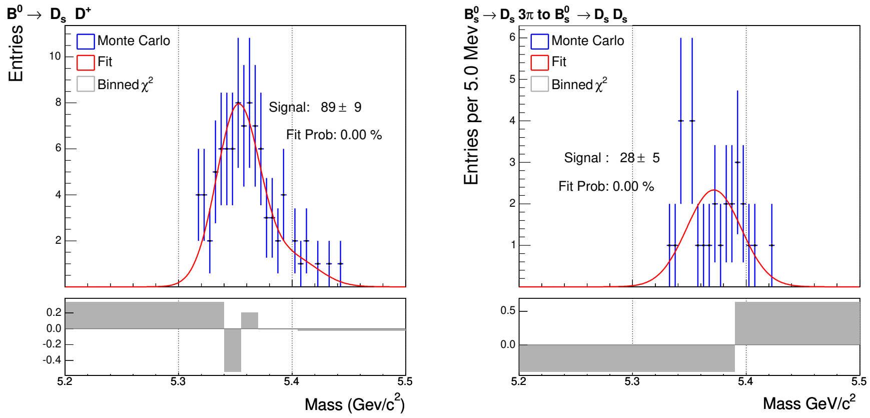

Figure 28: $B^0 \to D_s^+ D^-, D_s^+ \to \phi\pi$ template for $B_s \to D_s^+ D_s^-, (\phi\pi)(K^* K)$on the left and $B_s^0 \to D_s^+ 3\pi$ template for $B_s \to D_s^+ D_s^-, (\phi\pi)(\pi\pi\pi)$on the right.

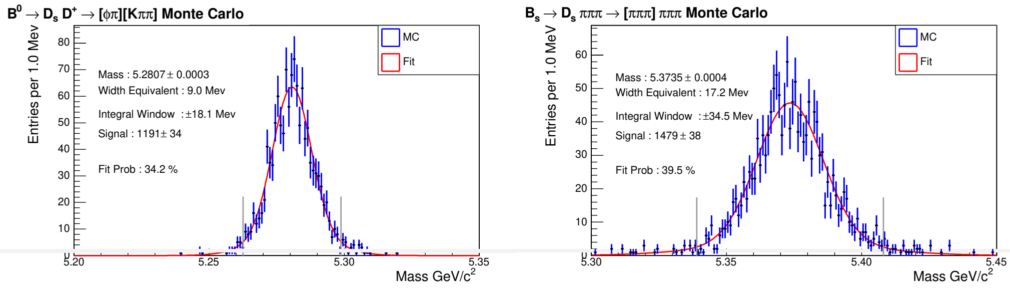

Figure 29: Reconstruction of $B^0 \to D_s^+ D^-, D_s^+ \to \phi\pi$ signal MC used for template above on the left. Reconstruction of $B_s^0 \to D_s^+ 3\pi$ signal MC used for template above on the right.

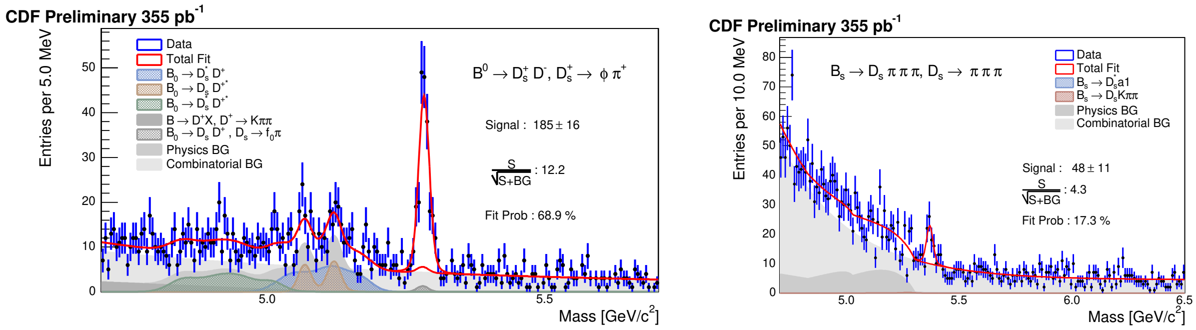

Figure 30: $B^0 \to D_s^+ D^-, D_s^+ \to \phi\pi$ and $B_s^0 \to D_s^+ 3\pi, D_s \to \pi\pi\pi$ data reconstruction.

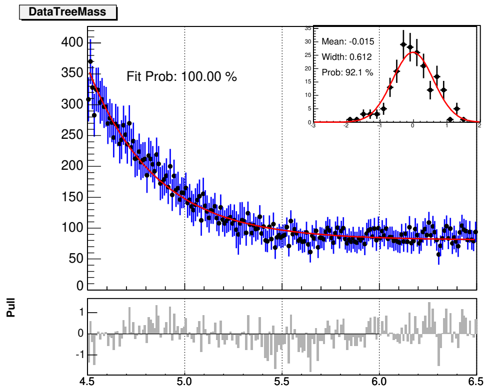

Figure 31: Templates for combinatorial background. Candidates with worng charge assignment are used.

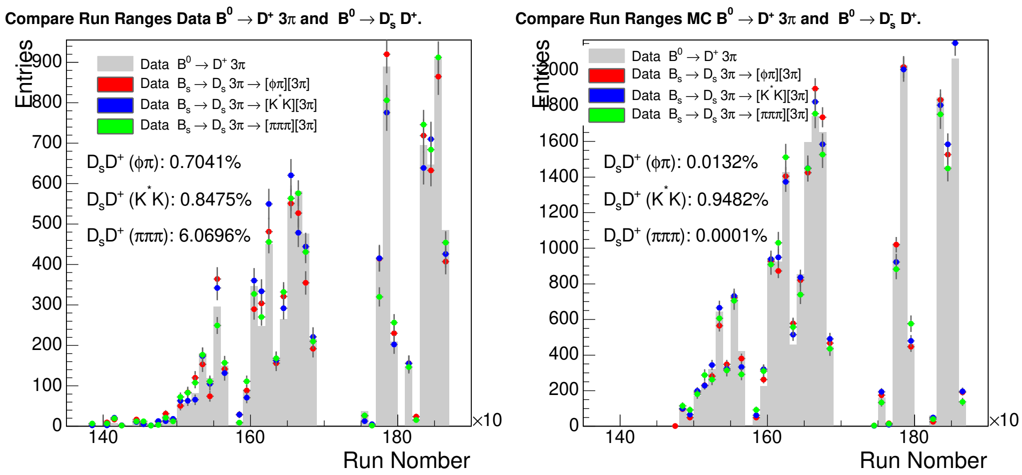

Figure 32: Comparing the run ranges for all four modes for Data and for Monte Carlo.

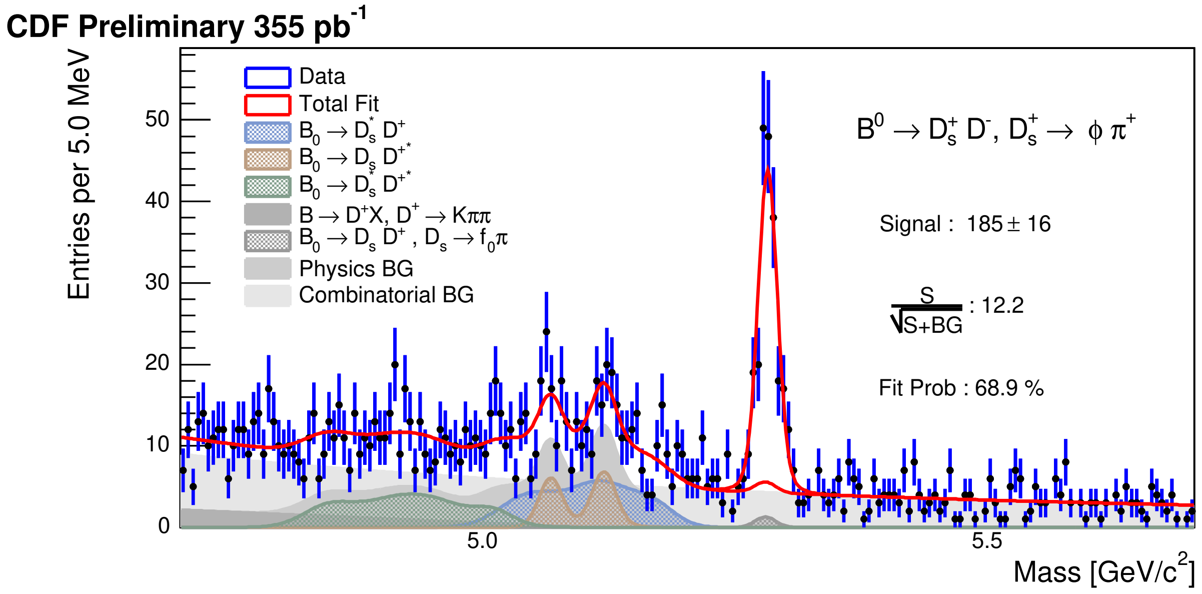

Figure 33: Reconstructed $B^0 \to D_s^+ D^-, D_s^+ \to \phi\pi$mass distribution.

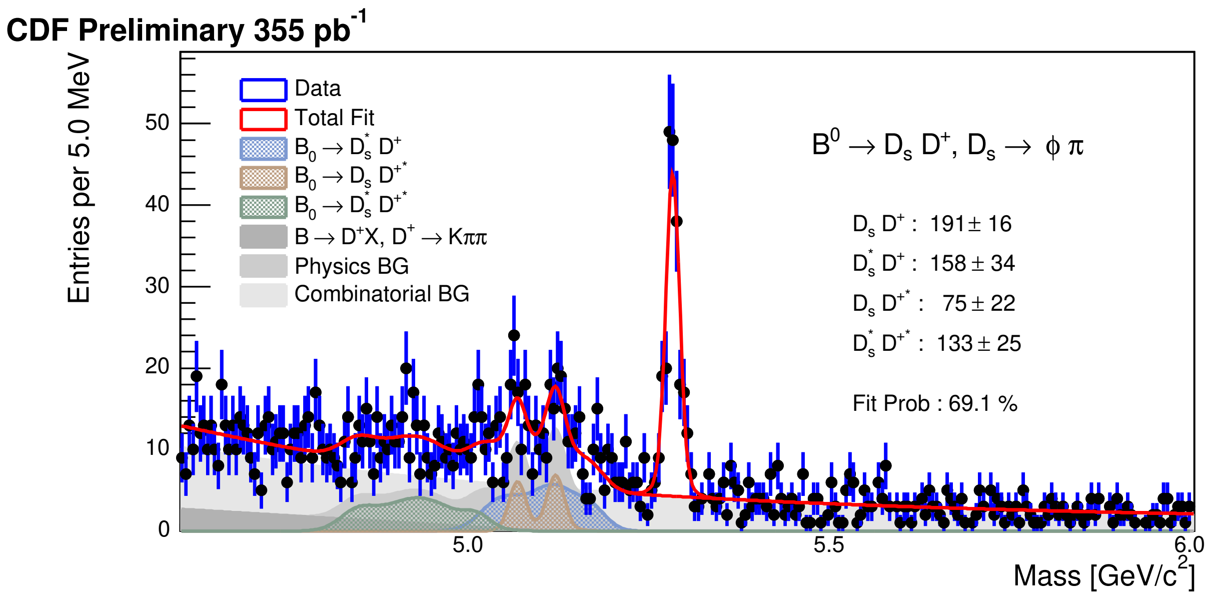

Figure 34: Reconstructed $B^0 \to D_s^+ D^-, D_s^+ \to \phi\pi$ mass distribution. The yields for $B^0 \to D_s^{+(*)} D^{-(*)}$modes are printed with errors.

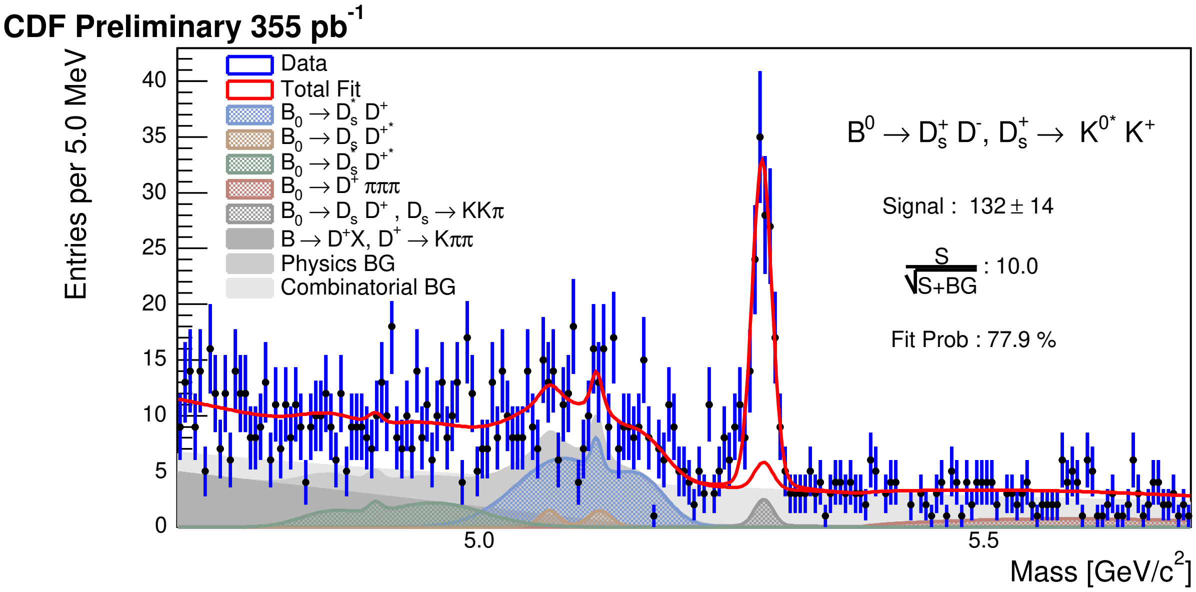

Figure 35: Reconstructed $B^0 \to D_s^+ D^-, D_s^+ \to K^* K$mass distribution.

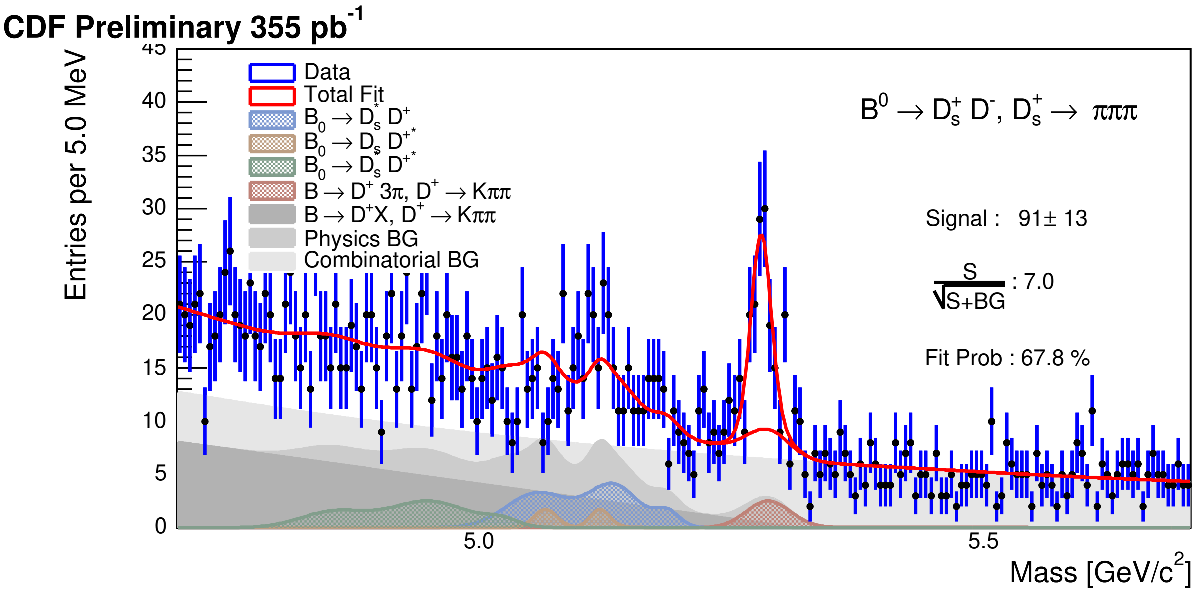

Figure 36: Reconstructed $B^0 \to D_s^+ D^-, D_s^+ \to \pi\pi\pi$mass distribution.

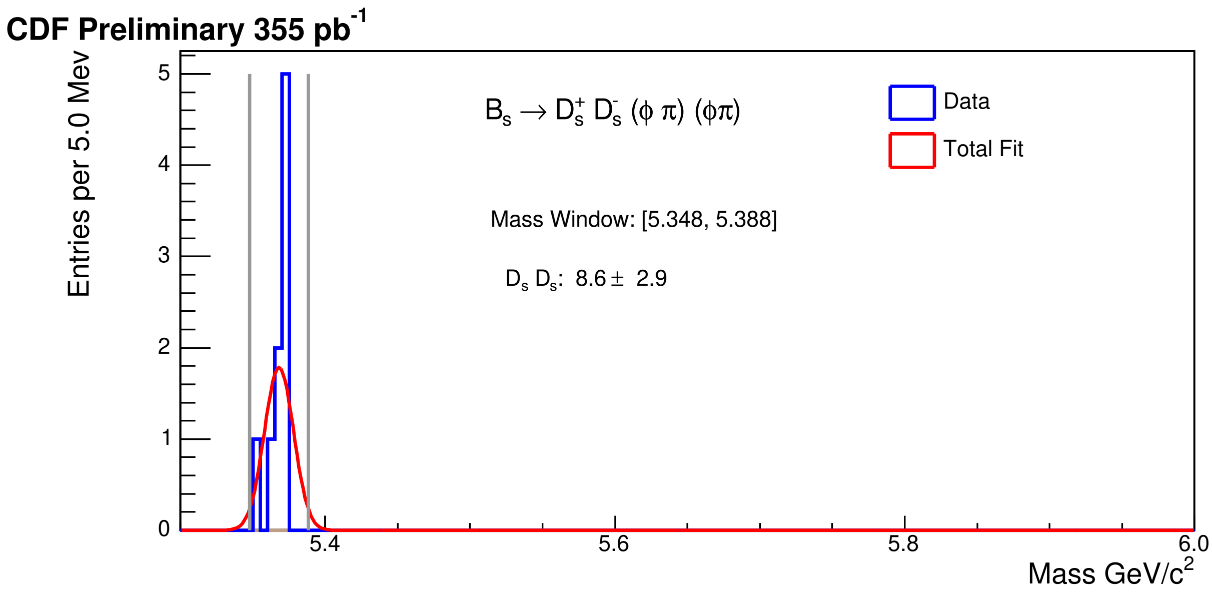

Figure 37: Reconstructed $B_s \rightarrow\ D_s^+ D_s^-, (\phi\pi)(\phi\pi)$mass distribution.

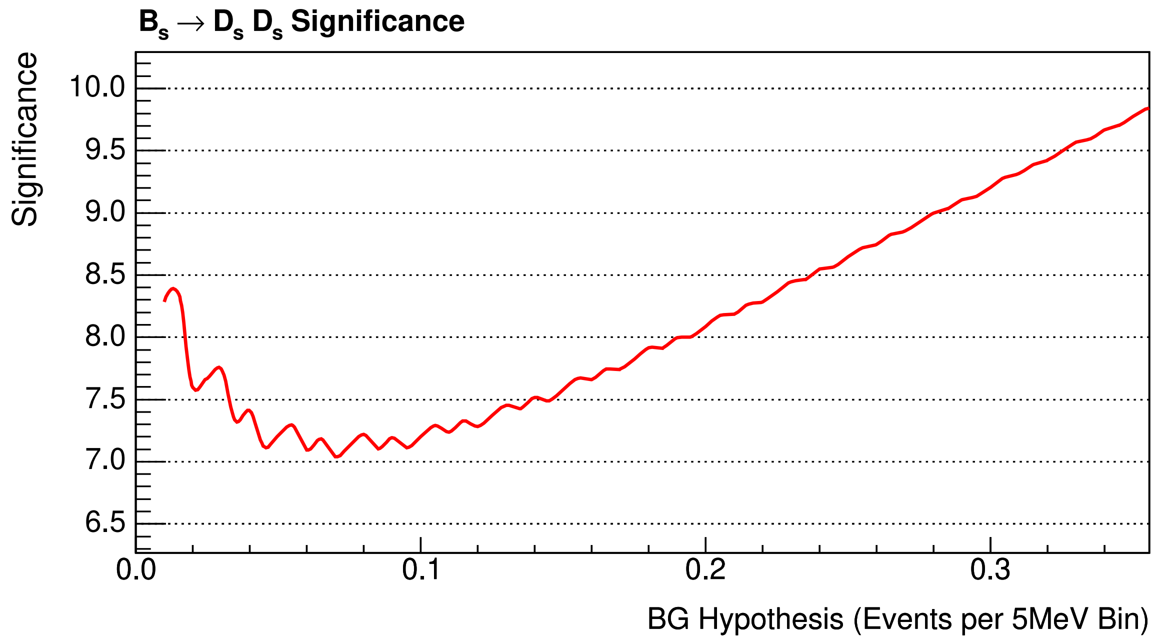

Figure 38: Significance of $B_s \rightarrow\ D_s^+ D_s^-, (\phi\pi)(\phi\pi)$signal.

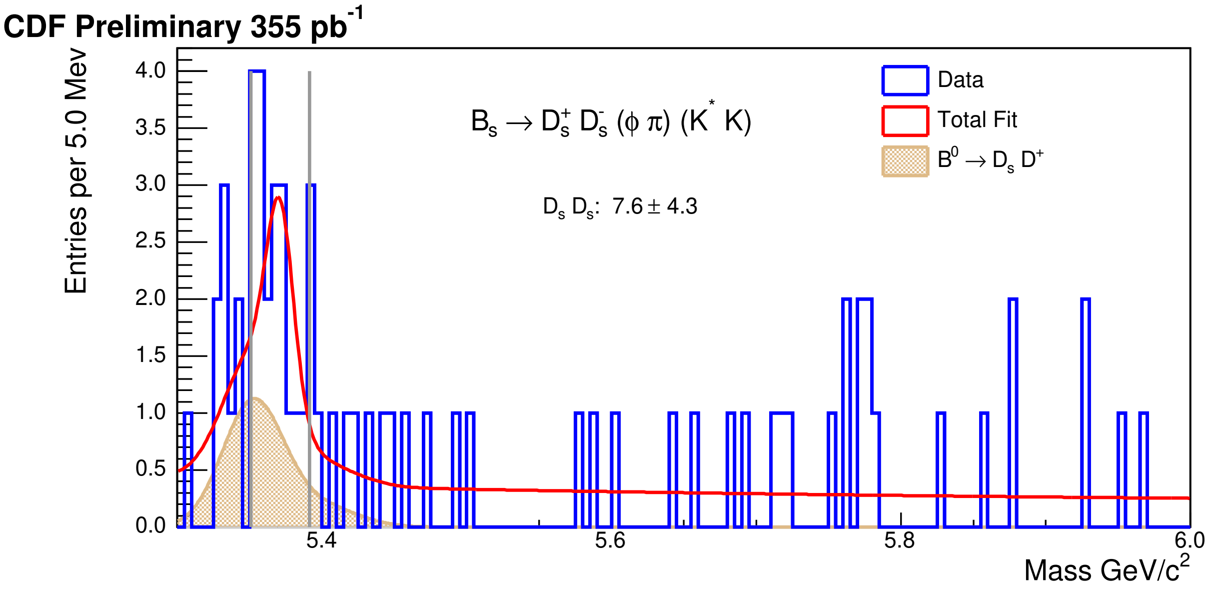

Figure 39: Reconstructed $B_s \rightarrow\ D_s^+D_s^-, (\phi\pi)(K^*K)$mass distribution.

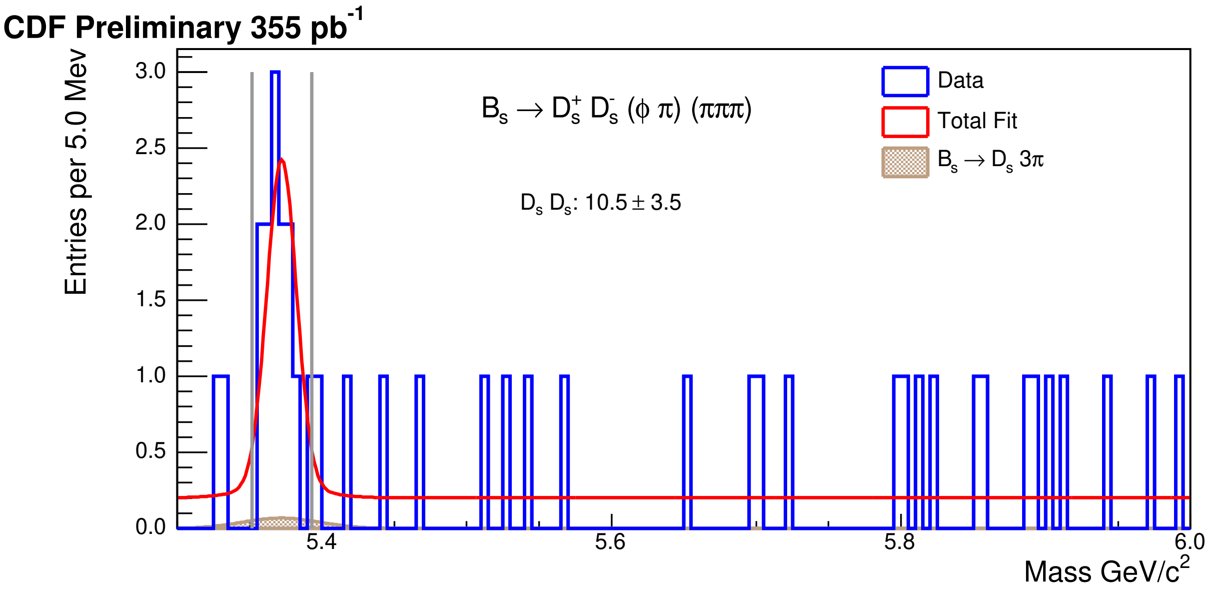

Figure 40: Reconstructed $B_s \rightarrow\ D_s^+D_s^-, (\phi\pi)(\pi\pi\pi)$mass distribution.

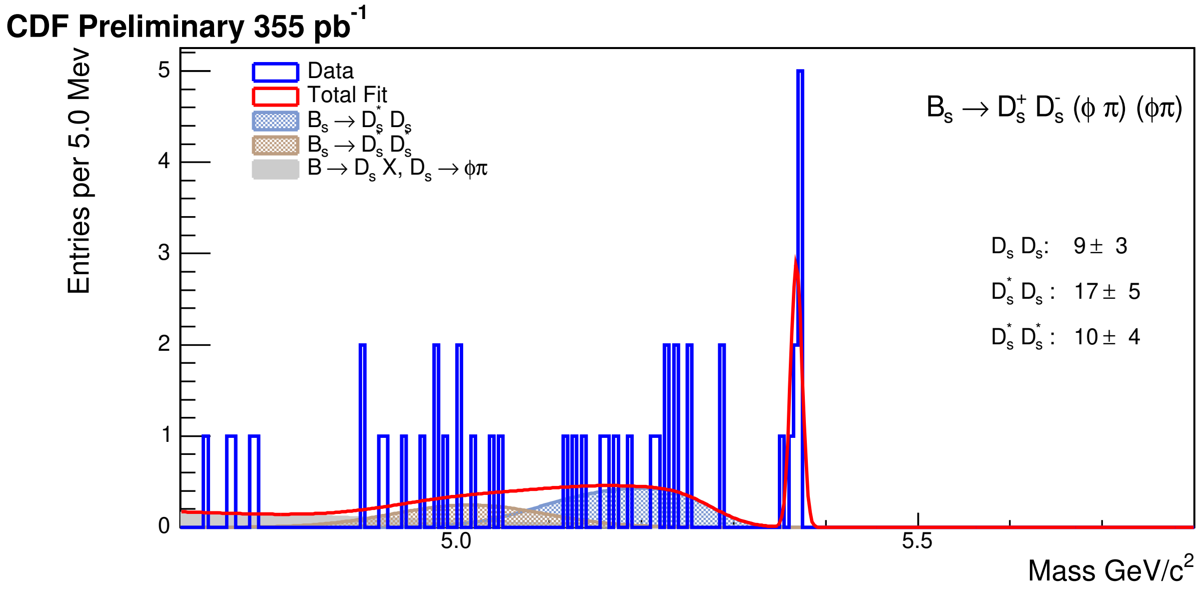

Figure 41: Reconstructed $B_s \to D_s^+ D_s^-, (\phi\pi)(\phi\pi)$mass distribution with fitted $B^0 \to D_s^{+(*)} D_s^{-(*)}$signals.

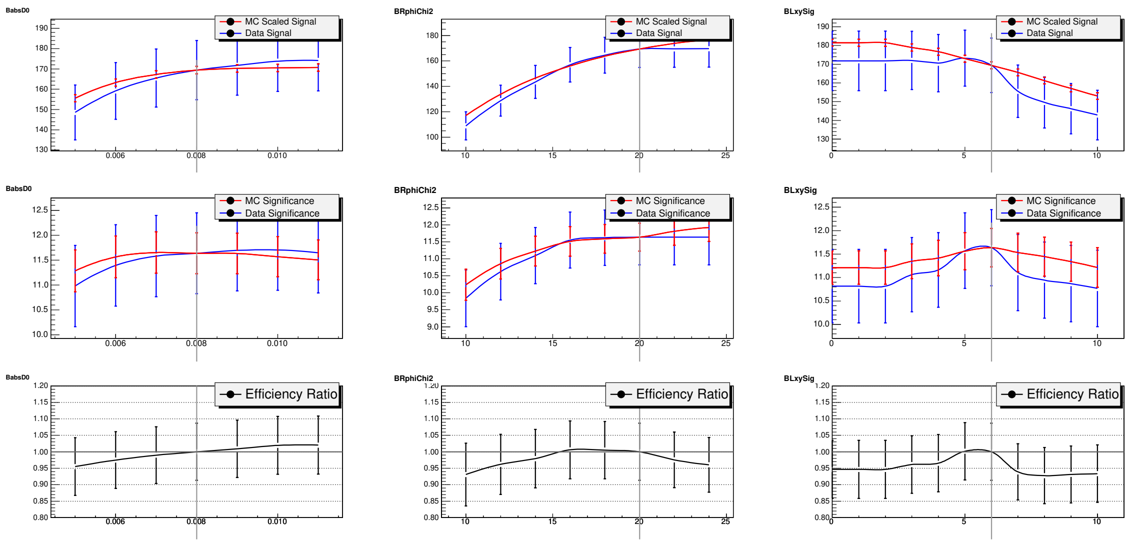

Figure 42: Cut systematics plots for $B^0 \to D_s^+ D^-, D_s^+ \to \phi\pi$: L_{xy} significance of the B, impact parameter of the B, and 2D χ^2 of the$B$ for `B_CHARM` and `LOWPT` combined Top plots show number of Monte Carlo scaled signal events, bottom plots - significance $\sigma = S/\sqrt{S+B}$ of the scaled Monte Carlo signal.

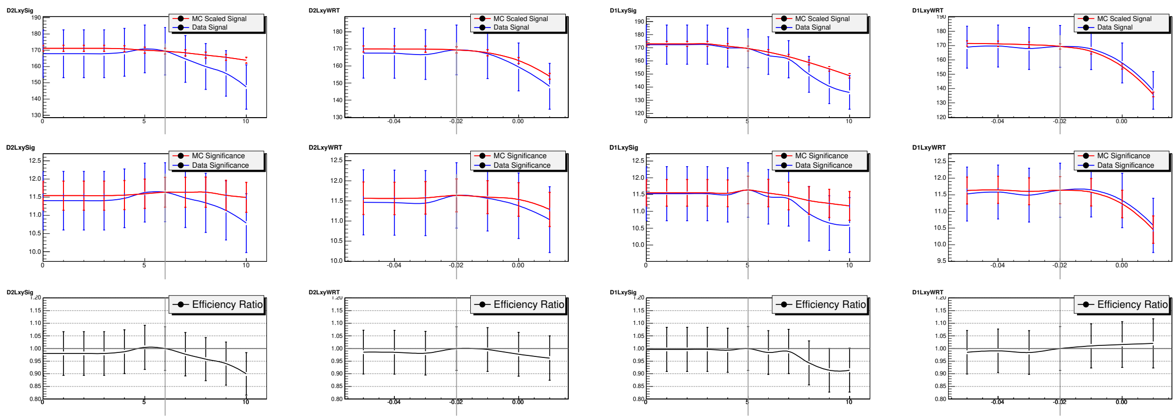

Figure 43: Cut systematics plots for $B^0 \to D_s^+ D^-, D_s^+ \to \phi\pi$: L_{xy} significance of the D^+, L_{xy} of the D^+ with respect to B, L_{xy} significance of the D_s, L_{xy} of the D_s with respect to B. Top plots show number of Monte Carlo scaled signal events, bottom plots - significance $\sigma = S/\sqrt{S+B}$ of the scaled Monte Carlo signal.